Nuclear Envelope Lamin-A Couples Actin Dynamics with Immunological Synapse Architecture and T Cell Activation

José María González-Granado,[1*] Carlos Silvestre-Roig,[1†] Vera Rocha-Perugini,[2,3†] Laia Trigueros-Motos,[1] Danay Cibrián,[2,3] Giulia Morlino,[2,3] Marta Blanco-Berrocal,[1] Fernando Garcia Osorio,[4] José María Pérez Freije,[4] Carlos López-Otín,[4] Francisco Sánchez-Madrid,[2,3*] Vicente Andrés[1*]

[1]Department of Epidemiology, Atherothrombosis and Imaging, Centro Nacional de Investigaciones Cardiovasculares (CNIC), Madrid, Spain. [2]Vascular Biology and Inflammation. CNIC, Madrid, Spain. [3]Servicio de Inmunología, Hospital de la Princesa, Instituto de Investigación Sanitaria Princesa, Madrid, Spain. [4]Departamento de Bioquímica y Biología Molecular, Universidad de Oviedo-IUOPA, Oviedo, Spain.

[*]Corresponding author. E-mail: jmagonzalez@cnic.es (J.-M.G.-G.); fsanchez.hlpr@salud.madrid.org (F.S.-M.); vandres@cnic.es (V.A.)

[†]These authors contributed equally to this work.

Abstract

In many cell types, nuclear A-type lamins have structural and functional activities, including higher-order genome organization, DNA replication and repair, gene transcription, and signal transduction; however, their role in specialized immune cells remains largely unexplored. Here, we showed that the abundance of A-type lamins was almost negligible in resting naïve T lymphocytes, but was increased upon activation of the T cell receptor (TCR). The increase in lamin-A was an early event that accelerated formation of the immunological synapse between T cells and antigen-presenting cells. Polymerization of F-actin in T cells is a critical step for immunological synapse formation, and lamin-A interacted with the linker of nucleoskeleton and cytoskeleton (LINC) complex to promote F-actin polymerization. Loss of lamin-A led to impaired TCR clustering and downstream signaling, including a reduction in extracellular signal–regulated kinase 1/2 (ERK1/2) signaling, and target gene expression. Pharmacological inhibition of the ERK pathway reduced lamin A–dependent T cell activation. Moreover, mice

deficient in lamin-A exhibited impaired T cell responses in vivo. These findings underscore the importance of A-type lamins for TCR activation, and identify lamin-A as a previously unappreciated regulator of the immune response.

Introduction

Mammalian A-type lamins, which include lamin-A and lamin-C and are encoded by the *LMNA* gene, are type V intermediate filaments of the nuclear envelope. In addition to their well-established role in maintaining the mechanical stability of the nucleus, A-type lamins and associated nuclear envelope proteins regulate higher-order chromatin organization, DNA repair and replication, nuclear positioning, signal transduction, gene transcription, as well as cell proliferation, differentiation, and migration (*1*, *2*). A-type lamins maintain cellular structural integrity not only by forming a complex network in the nucleus but also by bridging the nucleus and the plasma membrane through the LINC (linker of nucleoskeleton and cytoskeleton) complex, which contains nesprin and SUN (for Sad1p, UNC-84) proteins that connect the nuclear lamina with the cytoskeleton (*3*-*5*).

Lamin-A and lamin-C are found in most differentiated somatic cells; however, previous studies yielded no consensus about whether A-type lamins are found in immune cells, with some studies reporting a lack of lamin-A/C abundance (*6*-*9*) and others reporting their presence in lymphocytes (*10*-*13*) and human $CD4^+$ T cells (*14*). Moreover, although $Lmna^{-/-}$ mice, which are deficient in A-type lamins, exhibit severe age-dependent defects in thymic T cell development and in the numbers of T and B cells in lymphoid organs, these defects have been associated with the indirect effects of the loss of A-type lamin function in non-immune cells rather than a direct

effect in lymphocytes (*15*). Thus, the role of A-type lamins in T cell–mediated immune responses remains unclear.

T cells are activated upon presentation of specific antigens by antigen-presenting cells (APCs). This process involves the formation of the immunological synapse, a highly organized structure formed at the contact site between the T cell and the APC that favors transient cell-cell communications (*16-19*). Immunological synapse formation involves extensive spatial and temporal regulation of protein complexes to coordinate and tune signaling events. Upon activation, complexes of the T cell receptor (TCR) and CD3, and co-stimulatory receptors are concentrated at the central supramolecular activation cluster (cSMAC), which is surrounded by a peripheral SMAC (pSMAC), which is a ring of actin and integrins. The microtubule-organizing center (MTOC) is then directed to the center of the immunological synapse, thus polarizing the Golgi apparatus for directed secretion of granules (*20-22*). Both processes are critical for full T cell activation, as well as immunological synapse formation and maintenance (*20*). In addition, reorganization of the immunological synapse in T cells is associated with the recruitment and activation of intracellular pools of signaling molecules (*20*).

Here, through in vitro and in vivo studies, we provided evidence that suggests that A-type lamins are transiently increased in abundance in T cells upon antigen recognition, and we demonstrated that lamin-A is an important modulator of the threshold for activation of T cells by linking processes at the plasma membrane, cytoplasm, and nucleus.

Results

Lamin-A and lamin-C are transiently increased in abundance upon T cell activation

To investigate the expression of the gene encoding A-type lamins before and after T cell activation, we analyzed human peripheral blood lymphocytes (PBLs) and T lymphoblasts as well as mouse splenocytes and T lymphoblasts (fig. S1). We first analyzed primary immune cells from mice or human donors by confocal microscopy to detect A-type lamins. We found that lamin-A and lamin-C (collectively referred to hereafter as lamin-A/C) were detectable in only a small fraction of $CD4^+$ T cells in preparations of human PBLs and mouse splenocytes (Fig. 1A), whereas we detected B-type lamins in all $CD4^+$ T cells (fig. S2A). Flow cytometric studies demonstrated that lamin-A/C proteins were present in less than 10% of $CD4^+$ T cells from human peripheral blood (Fig. 1B).

To assess whether T cell activation resulted in increased lamin-A/C abundance, we analyzed the amounts of these proteins before and after TCR activation in PBLs and T lymphoblasts from humans and mice. Flow cytometry, confocal microscopy, and Western blotting analyses showed a transient and marked increase in lamin-A/C abundance upon TCR activation with *Staphylococcus* enterotoxin E (SEE) (Fig. 1C), SEE-loaded Raji cells (a human B lymphoblastoid cell line), SEE-loaded dendritic cells (DCs) (fig. S2B), or phytohemagglutinin (PHA) (Fig.1D). Consistent with these findings, $CD4^+$ T lymphoblasts from OTII transgenic mice bearing OTII TCRs specific for the ovalbumin (OVA) antigen displayed enhanced lamin-A/C abundance upon activation with OVA-loaded DCs (Fig. 1E).

To further investigate the time course of the increase in lamin-A/C abundance upon T cell activation, we performed quantitative, reverse transcriptase quantitative polymerase chain

reaction (qRT-PCR) and Western blotting analyses of human T lymphoblasts at different times after stimulation with Raji cells alone (which served as a negative control) or SEE-loaded Raji cells. Previous studies showed that APC–T cell interactions predominantly occur between 5 and 24 hours after exposure of T cells to antigen-presenting DCs (*23*-*26*). Compared with that in T cells incubated with Raji cells alone, *LMNA* mRNA abundance in T cells activated with SEE-loaded Raji cells was increased, with a peak at 4 hours after stimulation (fig. S2C), which was followed by the accumulation of lamin-A/C protein (fig. S2D). Appropriate T cell activation after their stimulation with SEE-loaded Raji cells was confirmed by detection of a marked increase in the amounts of mRNAs for the T cell activation markers *interleukin-2 (IL-2)* and *CD25*, which was not observed in cells stimulated with Raji cells alone (fig. S2E). Together, these data suggest that A-type lamins are rapidly and transiently increased in abundance upon activation of T cells through antigen presentation.

Lamin-A and lamin-C are required for optimal activation of T cells in vitro and in vivo

We next investigated whether A-type lamins regulated T cell function. Compared with wild-type splenocytes, those from *Lmna*$^{-/-}$ mice, which lack lamin-A/C proteins, had markedly reduced abundance of *CD25* mRNA upon stimulation in vitro with anti-CD3 and anti-CD28 antibodies, phorbol myristate acetate (PMA) and ionomycin (a calcium ionophore), or concanavalin A (Fig. 2A). Similarly, CD4^{+} T cells isolated from the spleens of *Lmna*$^{-/-}$ mice and stimulated with anti-CD3 and anti-CD28 antibodies displayed a substantial reduction in the cell-surface abundances of the T cell activation markers CD69 and CD25, as observed by flow cytometric analysis (Fig. 2B). Moreover, compared with wild-type controls, CD4^{+} T cells from OTII transgenic mice

lacking lamin-A/C (*Lmna*$^{-/-}$ OTII mice) displayed reduced cell-surface CD25 abundance upon stimulation with OVA-loaded DCs (Fig 2C).

To assess the role of lamin-A/C proteins as regulators of the immune response in vivo, we used a hapten-induced contact hypersensitivity (CHS) model (*27*). The immune response in this model starts with the application of the hapten oxalazone to the ear skin of mice, which triggers a sensitization phase during which specific T cells proliferate and migrate out of the lymph node upon recognition of hapten-carrier complexes presented by APCs. After re-exposure of the mice to oxalazone, an elicitation phase is initiated during which specific $CD4^+$ and $CD8^+$ T cells are activated in the dermis and trigger the inflammatory process (*27, 28*). As expected, we found that the elicitation phase after application of oxalazone to the ears of wild-type mice induced the progressive recruitment of $CD4^+$ T cells to the draining cervical lymph nodes over a period of 3 days (fig. S3, top). Furthermore, $CD4^+$ T cells recruited to lymph nodes in wild-type mice after challenge with oxalazone showed increased lamin-A/C abundance, with a peak at 2 days after challenge (fig. S3, bottom).

To investigate whether this increase in lamin-A/C abundance played any role in this model, we performed studies with lethally-irradiated wild-type mice transplanted with bone marrow cells from either wild-type mice or *Lmna*$^{-/-}$ mice. Irradiation and reconstitution was used to avoid any potential interference from non-immune cells and from the defects in T cell and B cell development that have been reported to occur in the thymus and spleen of *Lmna*$^{-/-}$ mice (*15*). Ear inflammation increased in both groups of mice during the first 2 days after challenge with oxalazone and then was progressively reduced (Fig. 2D). However, ear swelling was

substantially reduced at all of the time points analyzed in mice reconstituted with immune cells lacking lamin-A/C (Fig. 2D). To assess whether the reduced response observed in mice reconstituted with bone marrow cells from *Lmna*$^{-/-}$ mice was a result of decreased numbers of CD4^{+} T cells in the ears, we performed adoptive transfer of naïve CD4^{+} T cells from CD45.2^{+} wild-type or CD45.2^{+} *Lmna*$^{-/-}$ mice into recipient CD45.1^{+} wild-type mice. Oxazolone was then applied to the abdomens of the recipient mice, and we quantified the percentages of CD4^{+} T cells in the ears three days after the second application of oxalazone to the ears. We found that the percentages of transferred *Lmna*$^{-/-}$ CD45.2^{+} CD4^{+} T cells in the ears of recipient mice were reduced compared to those of transferred wild-type CD45.2^{+} CD4^{+} T cells (Fig. 2E).

We next performed competition experiments by adoptively transferring a 1:1 mixture of naïve CD4^{+} T cells from CD45.1^{+}CD45.2^{+} wild-type and CD45.2^{+} *Lmna*$^{-/-}$ mice into CD45.1^{+} wild-type recipient mice (Fig. 2F). Under these conditions, the numbers of transferred CD45.2^{+} *Lmna*$^{-/-}$ T cells that accumulated in the ears, lymph nodes, and spleens of recipient CD45.1^{+} wild-type mice were reduced compared to those of the transferred CD45.1^{+} CD45.2^{+} wild-type T cells (Fig. 2F). The reduction in the percentage of transferred *Lmna*$^{-/-}$ CD4^{+} T cells in the spleen (Fig. 2F) suggests that the absence of lamin-A/C might affect T cell proliferation upon recognition of the hapten. Together, these results demonstrate that loss of lamin-A/C in the mouse impairs T cell responses in vitro and in vivo.

To assess whether lamin-A enhanced the activation of human T cells, we performed gain-of-function studies with J77 cells, a human Jurkat T cell line derivative that does not have detectable endogenous *LMNA* mRNA or protein under basal conditions and which failed to

exhibit increases in *LMNA*mRNA abundance upon activation with SEE-pulsed Raji cells (fig. S4, A and B). As expected, J77 cells stably expressing GFP (J77-GFP cells) (fig. S4C) were activated upon incubation with SEE-loaded Raji cells compared with control J77-GFP cells incubated with non-loaded Raji cells, as determined by detection of increased amounts of *CD69* and *CD25* mRNAs (Fig. 3A) and the increased cell-surface abundance of CD69 (Fig. 3B). Moreover, J77 cells stably expressing GFP–Lamin-A (J77-GFP-Lamin-A; fig. S4, C and D) that were incubated with SEE-loaded Raji cells showed enhanced activation when compared to conjugated J77-GFP cells, as revealed by the presence of increased amounts of *CD69* and *CD25* mRNAs (Fig. 3A) and increased cell-surface abundance of CD69 (Fig. 3B). Treatment with anti-CD3 and anti-CD28 antibodies also enhanced the cell-surface abundance of CD69 on J77-GFP-Lamin-A cells compared to that on J77-GFP cells (Fig. 3C). Moreover, transient expression of dsRED-Lamin-A increased the cell-surface abundance of CD69 in J77-GFP cells incubated with SEE-loaded Raji cells compared to that on J77-GFP cells transfected with plasmid expressing dsRED alone (fig. S4E).

A-type lamins accelerate T cell–APC interaction dynamics and TCR-CD3 mobility in the plasma membrane and modulate TCR signaling

We next sought to elucidate the mechanisms through which A-type lamins enhanced T cell activation. Immunological synapse formation and T cell activation are finely regulated processes that entail multiple changes in the plasma membrane, cytoplasm, and nucleus (*20*). We hypothesized that lamin-A/C could regulate immunological synapse formation, orchestrating different processes required for T cell activation. To assess this possibility, we studied the effect of lamin-A on T cell–APC interactions and on the movement of molecules involved in

immunological synapse formation. J77-GFP or J77-GFP-Llamin-A cells were incubated with non-loaded or SEE-loaded Raji cells for different times and then were plated onto poly-L-lysine (PLL)-coated coverslips for immunofluorescence analysis. These studies revealed that J77-GFP-Lamin-A cells formed a greater percentage of conjugates than did J77-GFP cells at all of the time points analyzed (Fig. 4A), suggesting that lamin-A facilitates and stabilizes the formation of T cell–APC interactions.

To study this in more detail, we examined immunological synapse formation by time-lapse confocal microscopy (Fig. 4B and movie 1). Stably-transfected J77 cell lines were stained with different fluorescently labeled dyes and then were added on top of SEE-loaded Raji cells that had been stained with the cell tracker CMAC (7-amino-4-chloromethylcoumarin) and then allowed to attach to PLL–coated coverslips. We did not observe any differences in the times it took the J77-GFP and J77-GFP-Lamin-A cells to reach the focal plane (Fig. 4C). However, compared with J77-GFP controls, J77-GFP-Lamin-A cells formed more conjugates with SEE-loaded Raji cells at all of the time points tested (Fig. 4D), and these interactions were protracted (Fig. 4E).

After TCR engagement, TCR-CD3 complexes and co-stimulatory receptors accumulate at the cSMAC before being internalized (*20*). To study the effect of A-type lamins on the dynamic redistribution of receptors and co-receptors at the plasma membrane, we analyzed J77 cells transiently co-transfected with plasmids encoding CD3ζ-EGFP and either dsRED or dsRED-Lamin-A. GFP-rich populations were obtained by cell-sorting (fig. S5A) and then were activated by being plated onto coverslips coated with anti-CD3 antibody. Although the stimulating ligand was immobile on the glass and the TCR microclusters remained stationary, under these

conditions, there is protein flux into and out of the assembled clusters (*29, 30*). We then analyzed activated cells by total internal reflection fluorescence (TIRF) microscopy at a penetration depth of ~90 nm, which enabled the observation of CD3 microclusters at the plasma membrane (Fig. 5A). At the initial time points, J77-dsRED-Lamin-A cells exhibited an increased number of CD3-containing microclusters and a larger cSMAC area than did J77-dsRED cells, and these parameters were progressively reduced over time in both cell types (Fig. 5, B and C; movie 2).

We noted that the disappearance of CD3-containing microclusters from the TIRF detection depth range was faster in J77-dsRED-Lamin-A cells than in J77-dsRED cells (Fig. 5D), which suggested increased internalization. Accordingly, confocal microscopic analysis of J77-GFP-Lamin-A cells 30 min after conjugation with SEE-loaded Raji cells revealed that they had smaller cSMAC diameters and reduced numbers of CD3-containing microclusters at the membrane contact area compared to those of J77-GFP control cells (fig. S5, B and C). These results, which suggest that the presence of lamin-A accelerates both the dynamic redistribution of CD3 at the contact area during immunological synapse maturation as well as concomitant CD3 internalization, prompted us to investigate the effects of the presence of lamin-A on different signaling pathways downstream of TCR-CD3 activation. Western blotting analysis of J77-GFP-lamin-A cells conjugated for different times with SEE-loaded Raji cells revealed increased amounts of phosphorylated (activated) Vav1, myosin IIA, and extracellular signal–regulated kinase 1 (ERK1) and ERK2 (ERK1/2) compared to those of similarly treated J77-GFP cells (Fig. 5E). Moreover, treatment with the ERK1/2 inhibitor U0126 substantially reduced the cell-surface amount of CD69 in J77-GFP cells and J77-GFP-lamin-A cells conjugated with SEE-loaded Raji cells, and almost blunted the increase in CD69 abundance elicited by lamin-A (Fig. 5F).

A-type lamins promote MTOC translocation and F-actin polymerization in activated T cells

We hypothesized that differences in lamin-A/C–dependent signaling in activated T cells might be related to changes in the tubulin and actin cytoskeleton. To address this possibility, we first examined the translocation of the MTOC toward the immunological synapse, an important step in lymphocyte activation initiated by TCR signaling (*31*). Immunofluorescence and confocal microscopy revealed that the MTOC translocated faster to the immunological synapse in J77-GFP-Lamin-A cells than in control J77-GFP cells (Fig. 6A). Moreover, J77-GFP-Lamin-A cells exhibited increased F-actin polymerization induced by anti-CD3 and anti-CD28 antibodies, as measured by flow cytometric analysis of phalloidin-stained cells (Fig. 6B), as well as increased F-actin relocalization to the immunological synapse with respect to the rest of the membrane in cells conjugated with SEE-loaded Raji cells, as detected by confocal microscopy (Fig. 6C). Accordingly, human primary lamin-A/C–expressing T lymphoblasts subjected to knockdown of lamin-A/C by small inhibitory RNA (siRNA) (Fig. 6D) exhibited reduced F-actin polymerization upon stimulation with SEE-loaded Raji cells (Fig. 6E) or anti-CD3 and anti-CD28 antibodies (Fig. 6F). Together, these results indicate that A-type lamins promote F-actin polymerization and MTOC translocation during immunological synapse formation.

The lamin-A–mediated increase in T cell activation requires a physical connection between the nucleus and the cytoskeleton through the LINC complex

Together with nesprins and SUN proteins, lamin-A/C proteins mediate the connection between the nuclear lamina and the cytoskeleton (*3*-*5*). SUN proteins interact with lamin-A, and their

SUN domain extends into the perinuclear space to form contacts with the KASH (Klarsicht/Anc-1/SYNE homology) domains of nesprins, which are located at the outer nuclear membrane and connect with cytoplasmic microtubules, actin, and intermediate filaments (*4*, *5*). To assess whether these connections were required for optimal T cell activation and F-actin polymerization, we transfected J77-GFP-Lamin-A cells with plasmids encoding either a dominant-negative nesprin construct containing the C-terminal KASH domain fused to an N-terminal mCherry (DN KASH) (*32*), or a dominant negative SUN1 luminal domain construct (DN SUN) (*33*, *34*). Overexpression of these proteins disrupts the LINC complex and the connections between A-type lamins and the cytoskeleton (*32*). Consistent with our earlier results, we found that J77-GFP-Lamin-A cells conjugated with SEE-loaded Raji cells showed increased cell-surface expression of CD69 compared with J77-GFP cells (Fig. 7A), a response that was blunted upon overexpression of DN KASH (Fig. 7A). Furthermore, the presence of DN KASH did not affect CD69 cell-surface abundance in J77-GFP cells lacking lamin-A/C (Fig. 7A). Moreover, compared with cells transfected with control plasmids, J77-GFP-Lamin-A cells transfected with plasmids encoding DN KASH (Fig. 7B) or DN SUN (Fig. 7C) displayed reduced F-actin content upon stimulation with SEE-loaded Raji cells. Together, these results suggest that lamin-A–mediated increases in F-actin polymerization and T cell activation depend, at least in part, on the physical connection between the nucleus and the cytoskeleton mediated through physical interactions between lamin-A, SUN1, Nesprin, and the cytoskeleton.

Discussion

In this study, we provide evidence that A-type lamins are increased in abundance in T cells upon activation and that they mediate changes in signaling downstream of the TCR, in the actin

cytoskeleton, and in gene expression to increase the capacity of the cell to control the activation threshold. We also showed that the optimal stimulation of T cells elicited by A-type lamins required their physical connection with the cytoskeleton through nesprins and SUN proteins.

On the basis of previous studies (*6-9*), it was thought that lamin-A/C proteins are low in abundance (or undetectable) in hematopoietic cells (*5*). Our results demonstrate that A-type lamins are transiently present in T cells and that their abundance is controlled at the transcriptional level during TCR-mediated activation, consistent with other studies describing their expression in lymphocytes (*10-14*). A low degree of differentiation and a high degree of proliferation are associated with a reduction in the abundance of A-type lamins in normal cells and in human malignancies, including leukemias and lymphomas (*12, 35-38*). This loss of lamin-A proteins is associated with transcriptional silencing by the hypermethylation of CpG islands in the *LMNA* promoter in hematologic malignancies (*39*). Future studies are required to address the mechanisms that regulate lamin-A/C abundance in normal T cells.

Lmna$^{-/-}$ mice display severe age-dependent defects in T and B cell development (*15*). However, in irradiated wild-type mice reconstituted with bone marrow progenitor cells from *Lmna*$^{-/-}$ mice, T and B cells develop normally in the thymus, and normal immune cell populations are observed in the spleen (*15*). Furthermore, in irradiated wild-type mice that were infected with a lymphocytic choriomeningitis virus after reconstitution with a 1:1 mixture of wild-type and *Lmna*$^{-/-}$ bone marrow cells, T cells functioned normally in terms of their production of the cytokines IL-2, interferon-γ (IFN-γ), and tumor necrosis factor-α (TNF-α) (*15*). Our gain- and loss-of-function experiments demonstrate a direct effect of A-type lamins in T cell activation. In

vitro, ectopically expressed lamin-A enhanced T cell activation, whereas T cells from *Lmna*$^{-/-}$ mice showed impaired activation, as monitored by the reduced abundances of the activation markers CD69 and CD25 at both the mRNA and protein levels. A role for A-type lamins in T cell activation was further suggested by our in vivo studies with a mouse model of the contact hypersensitivity inflammatory response, in which transplantation of *Lmna*$^{-/-}$ bone marrow cells failed to reconstitute the inflammatory response in lethally-irradiated wild-type mice to the same extent as that achieved by transplantation with cells with intact A-type lamins. The results of the CD4^{+} T cell adoptive transfer experiments indicate that the impaired response observed in mice reconstituted with *Lmna*$^{-/-}$ bone marrow cells may have been a result of a reduction in the numbers of CD4^{+} T cells in the inflamed ears and their corresponding draining lymph nodes. Moreover, this reduction may have been related to a defect in cellular proliferation, because there was also a reduction in the numbers of *Lmna*$^{-/-}$ CD4^{+} T cells in the spleens of the recipient mice. Thus, our work, together with the study of Hale *et al.* (*15*), reveal the complexity of the role of A-type lamins in immune responses, which deserves further investigation.

It was unexpected that A-type lamins, which are confined to the nucleus, could regulate several events that control immunological synapse formation and T cell activation, functions that occur at the plasma membrane and in the cytoplasm. At the plasma membrane, engagement of the TCR results in the formation of signaling microclusters, which are enriched in receptors and co-receptors (such as the TCR and CD3), as well as kinases and adaptor proteins, which generate signaling events. Our results show that A-type lamins regulate several points of these complex pathways. We found that A-type lamins enhanced cytoplasmic F-actin polymerization upon TCR engagement, which may be an important factor in the regulation by A-type lamins of events that

take place outside the nucleus. Consistent with this observation, compared to wild-type cells, *Lmna*$^{-/-}$ mouse embryonic fibroblasts have a larger fraction of highly mobile cytoplasmic actin, reassemble stress fibers more slowly after disruption of actin filaments with cytochalasin D, and do not increase the ratio of F-actin to G-actin upon serum stimulation (*40*). Moreover, the actin cytoskeleton can localize many signaling proteins close to receptors, as well as generate barriers to restrict the movement of molecules (*41*), including CD3 microclusters (*42*). In this regard, we found that A-type lamins modified both the molecular density of CD3 at the membrane and its behavior upon TCR engagement. The movement of microclusters also depends on the activation of myosin IIA (*43-45*), which contributes to actin retrograde flow (*46*) and activates Vav1, which in turn promotes F-actin polymerization (*21, 44*). Our results showed that the presence of lamin-A enhanced the extent of phosphorylation of myosin IIA and Vav1, which could lead to increased F-actin polymerization and microcluster dynamics.

There is evidence that the accumulation of F-actin at the immunological synapse enhances signaling by providing a nanoscale scaffold for the assembly of signaling complexes, maintaining cell-cell contacts, and organizing cell polarity (*18, 42, 47*). In terms of cell-cell contacts, lamin-A increases the number and duration of contacts between T cells and APCs. These effects may be explained by increased formation of lamellipodia, which is augmented by F-actin polymerization and which helps the formation of a complete, functional immunological synapse (*48*). In terms of cell polarity, formation of an immunological synapse leads to the disassembly of the uropod at the back of the cell, as well as movement of the MTOC to a new position between the nucleus and the cell-cell contact surface at the front of the cell. These processes switch the axis of polarity towards the APC, which enables the endocytic and exocytic

apparatus to be configured to sustain the directed secretion of cytokines, exosomes, and cytotoxic granules at the cell-cell contacts (*49*, *50*). Polarization of the MTOC depends on phosphorylation of phospholipase C-γ1 (PLC-γ1) (*51*), which can be stimulated by F-actin polymerization (*52*). Our results showed that lamin-A stimulated F-actin polymerization and the subsequent activation of PLC-γ1, which may contribute to increased MTOC polarization. Lamin-A might also modify the actin and tubulin cytoskeleton by changing the degree of activation of other proteins involved in their remodeling, such as Vav1 and myosin IIA.

Lamin-A/C can also modulate T cell activation by provoking changes inside the nucleus, as demonstrated by the modifications in the abundances of *CD25* and *CD69* mRNAs upon the over-expression or knockdown of lamin-A and lamin-A/C, respectively. These changes can be attributed, in part, to alterations in signaling and gene expression, because A-type lamins interact with and regulate signaling proteins and transcription factors (*1*, *2*). Specifically, we found that lamin-A-expressing T cells exhibited increased phosphorylation of ERK1/2, which increases the cell-surface abundances of CD69 and CD25 (*53*-*58*). Indeed, pharmacological inhibition of ERK1/2 blunted the lamin-A-dependent increase in cell-surface CD69 abundance. The effect of lamin-A/C on ERK1/2 phosphorylation (activation) might result from their direct interaction with each other (*59*).

The nucleus is connected to the cytoskeleton by interactions between lamin-A, SUN proteins, and KASH domain–containing nesprins (*3*-*5*). Our experiments with DN KASH proteins indicated that nuclear-cytoskeletal connections involving these proteins were necessary for enhanced activation of J77-GFP-Lamin-A cells, as revealed by increased CD69 abundance.

Notably, DN KASH did not affect CD69 protein abundance in J77-GFP cells, which have endogenous lamin-B, but undetectable lamin-A/C. The most plausible explanation for this inability of lamin-B to compensate for the loss of lamin-A/C is the absence of any interaction between lamin-B and SUN proteins (*34*). Moreover, the reduced F-actin content observed when DN KASH and DN SUN proteins were expressed in J77-GFP-Lamin-A cells suggests that lamin-A-dependent F-actin polymerization is mediated by nuclear-cytoskeletal connections.

The nuclear lamina is connected with the plasma membrane through interactions between the LINC complex, the cytoskeleton, and membrane-bound adhesion molecules, such as integrins (*60-62*), and these connections are essential for the ability of cells to sense and respond to external stimuli (*63*). In addition, the adhesion of lymphocytes to the extracellular matrix and other cells is mediated by integrins (*64*). By forming bridges between the cytoskeleton and the nucleus, lamin-A might therefore facilitate the conversion of mechanical signals from the plasma membrane into the activation of specific signaling pathways and the expression of mechanosensitive genes, a process known as mechanotransduction, which has been postulated as a means of regulating T cell activation (*65*). Our results suggest that the connections between the cytoskeleton and A-type lamins might provide T cells with an increased capacity to transmit mechanical forces from the membrane to the nuclear interior that are necessary for adequate modulation of T cell functions. Further research is necessary to investigate whether lamin-A regulates integrin-dependent signaling.

In summary, we demonstrated that A-type lamins are increased in abundance in T cells upon antigen recognition and that they are required for optimal T cell activation, by regulating directly

or indirectly several events that occur at the plasma membrane and in the cytoplasm and nucleus. We also showed that optimal T cell activation elicited by A-type lamins required a physical connection between the nuclear envelope and the cytoskeleton through the LINC complex.

Materials and Methods

Plasmids

The plasmids encoding mCherry and EGFP were purchased from Clontech. The plasmids encoding CD3ζ-EGFP (*66*), DN KASH (32), DN SUN (33, 34) dsRED and dsRED-Lamin-A (*67*), and EGFP-lamin-A (*68*) were previously described.

Cells and mice

Vβ8 Jurkat J77cl20 (J77) T cells, Vβ3 Jurkat (CH7C17) T cells, and lymphoblastoid Raji B cells were cultured in complete medium [RPMI 1640, 10% fetal bovine serum (FBS, Sigma)]. Human PBLs were isolated from freshly prepared buffy coats obtained from healthy donors. PHA-activated and SEE-specific human T lymphoblasts were obtained as described previously (*69*). When indicated, human T lymphoblasts were co-cultured with SEE-loaded monocyte-derived DCs, which were obtained as described previously (*70*). Stable J77 cell populations overexpressing GFP or GFP-Lamin-A were generated by transfection of plasmids encoding EGFP or EGFP-lamin-A, respectively, followed by selection with G418 (1 mg/ml, Invitrogen). *Lmna*$^{-/-}$ mice were previously described (*71*). C57BL/6-Tg (TcraTcrb)425Cbn/J mice (OTII mice) expressing a TCR specific for the OVA peptide (amino acid residues 323 to 339) in the context of I-Ab were purchased from the Jackson Laboratory (stock number 004194). *Lmna*$^{-/-}$

OTII mice were generated by crossing OTII mice with *Lmna*$^{-/-}$ mice. CD45.1^{+} B6.SJL mice were used as the recipients for adoptive transfers. CD45.1^{+}CD45.2^{+} wild-type mice were generated by crossing C57BL/6 CD45.2^{+} mice with C57BL/6 CD45.1^{+} mice. To obtain T lymphoblasts from wild-type and OTII mice, naïve CD4^{+} T cells (10^{6} cells/ml) were cultured in the presence of irradiated APCs (T cell-depleted splenocytes) and OVA peptide (10 μg/ml). After 1 day, cells were washed, and IL-2 (10 ng/ml) was added to the medium. Seven days later, irradiated APCs and OVA peptide (10 μg/ml) were added to stimulate the CD4^{+} T lymphoblasts.

Antibodies and reagents

Staphylococcus enterotoxin E (SEE) was purchased from Toxin Technology. The CellTracker Blue CMAC, Alexa Fluor 647-conjugated anti-α-tubulin antibody, Alexa Fluor 488-conjugated phalloidin, and Alexa Fluor 647-conjugated phalloidin were obtained from Invitrogen. Human fibronectin, PLL, anti-α-tubulin antibody, and U0126 were obtained from Sigma-Aldrich. Primary antibodies include SPV-T3b (anti-human-CD3) (*72*), TP1/55 (anti-human CD69) (*73*), and HP2/6 (anti-human CD4) (*74*). The monoclonal antibody specific for Vav1 phosphorylated at Tyr^{174} (pVav1 Y174) was a kind gift from X. Bustelo (Centro de Investigación del Cáncer, Salamanca). Anti-Vav and anti-ERK1/2 antibodies were from Millipore. Anti-phosphorylated MLC, anti-MLC, anti-lamin-A/C, anti-lamin-A, and anti-ERK2 antibodies were obtained from Santa Cruz Biotechnology. Anti–PLC-γ1 (Y783), anti–PLC-γ1, Alexa Fluor 488-conjugated anti-lamin-A/C, and Alexa Fluor 488-conjugated mouse immunoglobulin G1 (IgG1) isotype control were obtained from Cell Signaling. Allophycocyanin (APC)-conjugated anti-human CD69, fluorescein isothiocyanate (FITC)-conjugated anti-mouse CD69, anti-mouse CD3, anti-CD28, PerCPCy5.5-conjugated anti-CD45.1, Alexa Fluor 647-conjugated anti-CD45.1, anti-CD45.2-

V450, and biotinylated antibodies against B220, CD19, MHCII, CD11c, CD11b, CD44, and CD8α were from BD Biosciences.

Cell transfection and gene silencing

J77 cells or primary human T lymphoblasts (2×10^7 cells) were washed twice with Hanks' balanced salt solution (HBSS, Cambrex) and transiently transfected by electroporation with plasmids (20 µg) or 1 µM siRNA in OPTIMEM medium (Gibco, Invitrogen) at 240 V and 32 ms (Gene Pulser II, Bio-Rad). Plasmids encoding EGFP-lamin-A, dsRED, and dsRED-Lamin-A were used. Specific double-stranded siRNAs against human lamin-A/C or negative control siRNAs were purchased from Eurogentec. The efficiency of gene silencing was assessed by Western blotting, flow cytometric, and confocal microscopic analysis 24 hours after transfection.

Cell-cell conjugate formation

Raji cells were incubated with CMAC in HBSS for 30 min and then with or without SEE (0.5 µg/ml), centrifuged at low speed, washed, and then allowed to form conjugates with J77 cells or $CD4^+$ human T lymphoblasts obtained from SEE-treated PBLs at 37°C for the times indicated in the figure legends.

Flow cytometry

Cells were cocultured in 96-well plates at 37°C for the times indicated in the legends. After cells were incubated and stained with specific antibodies, data were acquired on FACSCantoII or LSRFortessa flow cytometers (BD Biosciences) and analyzed with BD FACSDIVA (BD Biosciences) or FlowJo (Treestar Inc) software. Raji cells were distinguished from other cells by

CMAC staining. To measure F-actin content, cells were stimulated for different times with purified anti-CD3 antibody (10 µg/ml, T3b) or SEE-loaded, CMAC-stained Raji cells, fixed in 2% paraformaldehyde (PFA), permeabilized with 0.5% Triton X-100, and labeled with phalloidin. For experiments in which ERK1/2 signaling was blocked, J77 cells were preincubated for 1 hour with the MEK1/2 inhibitor U0126 (which prevents the activation of ERK1/2), and then were allowed to form conjugates with Raji cells in the presence of the inhibitor for the times indicated in the figure legends.

Western blotting analysis

J77 cells were allowed to form conjugates with SEE-loaded Raji cells (at a ratio of 10:1) for the times indicated in the figure legends, after which they were lysed at 4°C for 40 min with 50 mM Tris-HCl (pH 7.5), 1% NP-40, 0.2% Triton X-100, 150 mM NaCl in phosphate-buffered saline (PBS) containing phosphatase and protease inhibitors (Roche). Cell lysates were centrifuged at 2500*g* for 10 min to remove cellular debris and nuclei. Whole-cell lysates were analyzed by SDS-polyacrylamide gel electrophoresis (SDS-PAGE), transferred to polyvinylidene difluoride (PVDF) membranes, and incubated with the appropriate primary antibodies in Tris-buffered saline, 1% Tween 20. Bound antibodies were detected with horseradish peroxidase -conjugated secondary antibodies, and membranes were developed by enhanced chemiluminescence with Super-Signal West Pico or Femto chemiluminescent substrate (Pierce Chemical). Band intensities were quantified with Metamorph software, and the intensities of bands of interest were normalized to those of the appropriate controls, for example, total proteins in the case of analysis of phosphorylated proteins.

Fluorescence confocal microscopy

Confocal images were obtained with a Leica TCS-SP5 confocal scanning laser unit attached to an inverted epifluorescence microscope (DMI6000B) and fitted with an HCX PL APO lambda blue 63X/1.4 oil immersion objective, or with a Zeiss LSM700 confocal scanning laser unit attached to an inverted epifluorescence microscope (Observer.Z1) fitted with a Pan APO Chromat 63X/1.4 oil immersion objective. For live-cell imaging, microscopes are covered by a full acrylic box to enable analysis at 37°C, 5% CO_2. For time-lapse fluorescence imaging, cells were resuspended in HBSS (Lonza), 2% FBS, 20 mM Hepes, and were plated onto PLL-coated 35-mm dishes (MatTek). Cells expressing GFP or GFP–Lamin-A were differentially stained with vibrant DiI and DiD cell labels (Invitrogen). Images were analyzed with Leica LASAF (Leica Microsystems), Metamorph (Molecular Devices) Imaris (Bitplane), or ImageJ (NIH) software. For immunofluorescence assays, cells were plated on slides coated with PLL (50 μg/ml) for 5 min at 37°C, fixed in 2% PFA-1% sucrose, incubated with the appropriate primary antibodies followed by species-matching secondary antibodies coupled to Alexa Fluor fluorochromes (Invitrogen), and then mounted in ProLong Gold antifade medium (Invitrogen). To detect intracellular proteins, cells were first permeabilized with 0.5% Triton X-100 for 5 min. F-actin accumulation at the immunological synapse was measured in three-dimensional (3D) confocal maximal projections with the Synapsemeasure plugin in ImageJ (*75*). In the charts, each dot corresponds to a T cell-B cell conjugate. The distance from MTOC to the contact area between a T cell and an APC was measured in 3D confocal maximal projections with ImageJ.

Quantitative RT-PCR analysis

Total RNA was isolated from mouse splenocytes or J77 cells with Qiazol Lysis Reagent (Qiagen) and isopropanol precipitation or with the RNeasy Mini kit (Qiagen), according to the manufacturer's instructions. RNA concentration and purity were assessed from the ratio of absorbances at 260 and 280 nm, and RNA integrity was verified by separation on ethidium bromide-stained 1% agarose gels. Complementary DNA (cDNA) was generated from total RNA (0.1 to 1 µg per reaction) with the High Capacity cDNA Reverse Transcription Kit (Applied Biosystems) with random hexamers and RNase Inhibitor, according to the manufacturer's protocol. Quantitative PCR was performed with the ABI PRISM 7900HT Sequence Detection System (Applied Biosystems) with the PCR Power SYBR Green PCR Master Mix (Applied Biosystems), and reactions were performed in technical triplicates. The sequences of the forward and reverse primers used for RT-PCR are as follows. Mouse genes: *Cd69*: 5'-ATCTCTCCGTGGACCACTTG-3' and 5'-CACAGCCCAAGGGATAGAAA-3'; *Cd25*: 5'-AACAACTGCAATGACGGAGACAT-3' and 5'-CAGCTGGCCACTGCTACCTT-3'; *Hprt1*: 5'-CCTAAGATGAGCGCAAGTTGAA-3' and 5'-CCACAGGACTAGAACACCTGCTAA-3'. Human genes: *IL-2*: 5'-AAGTTTTACATGCCCAAGAAGG-3' and 5'-AAGTGAAAGTTTTGCTTTGAGC-3'; *CD69*: 5'-TCCGGAGAGTGGACAAGAAAAT-3' and 5'-GACCCTTCATGACGTGTTGAGA-3'; *CD25*: 5'-ACGGGAAGACAAGGTGGAC-3' and 5'-TGCCTGAGGCTTCTCTTCAC-3'; *LAMIN-A*: 5'-GACGAGGATGAGGATGGAGA-3' and 5'-GACACTGGAGGCAGAAGAGC-3'; *LAMIN-A*/C (recognizing both *LAMIN-A* and *LAMIN-C* mRNAs): 5'-ATGGAGATGATCCCTTGCTG-3' and 5'-CTTCTTCCCCAGTGGAGTTG-3'; *LAMIN-C*: 5'-CAACTCCACTGGGGAAGAAG-3' and 5'-AACATTCTTTAATGAAAAGATTTTTGG-3'; *HPRT1*: 5'-TGACACTGGCAAAACAATGCA-3' and 5'-GGTCCTTTTCACCAGCAAGCT-3'. The exent

of expression of a gene of interest was analyzed by the comparative Ct method with Biogazelle qBasePLUS software using as an internal control the housekeeping gene HPRT1 (hypoxanthine phosphoribosyltransferase 1). Results are represented as fold change relative to control conditions (see details in figure legends).

Generation of chimeric mice, adoptive transfer experiments, and contact hypersensitivity assays

C57BL6 wild-type recipient mice received 9.5 Gy of total body irradiation administered in two treatments from a ^{137}Cs source. Bone marrow cells from CD45.2$^+$ wild-type and CD45.2$^+$ *Lmna*$^{-/-}$ mice were transplanted into CD45.1$^+$ wild-type recipients by tail-vein injections immediately after irradiation (ten mice per group). Eight weeks after transplantation, the chimeric condition of the mice was assessed by flow cytometric analysis of blood cells stained with a combination of fluorescently labeled anti-CD45.1 and anti-CD45.2 antibodies to detect CD45.2$^+$ cells from donors and CD45.1$^+$ cells from recipient mice, which confirmed that more than 90% of the cells analyzed were derived from the transplanted bone marrow cells (fig. S6). For the adoptive transfer experiments, CD4$^+$ T cells from CD45.2$^+$ *Lmna*$^{-/-}$, CD45.1$^+$CD45.2$^+$ wild-type, or CD45.2$^+$ wild-type mice were isolated by negative selection from spleens with MACS separation columns (Miltenyi Biotec) after labeling the cells with a cocktail of biotinylated antibodies against B220, CD19, MHCII, CD11c, CD11b, CD44, and CD8α, as well as with a solution containing streptavidin-bound magnetic microbeads (Miltenyi Biotec). Adoptive transfer experiments were performed by inoculating CD45.1$^+$ wild-type recipient mice with 2×10^6 CD4$^+$ T cells from the spleen of CD45.2$^+$ *Lmna*$^{-/-}$ or CD45.2$^+$ wild-type mice or by inoculating CD45.1$^+$ wild-type recipient mice with 4×10^6 cells of a 1:1 mixture of CD4$^+$ T cells from the

spleens of $CD45.2^+$ *Lmna*$^{-/-}$ and $CD45.1^+CD45.2^+$ wild-type mice. In both cases, adoptive cell transfer was performed 24 hours before the first application of oxazolone. In mice transplanted with bone marrow cells as well as in adoptively transferred mice, contact hypersensitivity was induced by painting shaved mouse abdomen skin with 200 µl of 3% oxazolone (4-ethoxymethylene-2-phenyl-2-oxazolin-5-one, Sigma) in ethanol. After 5 days, mice were challenged with 20 µl of 1% oxazolone on each side of the right ear. The left ear was painted with vehicle as a control. In transplanted mice, ear thickness was measured in a blinded manner every day for 7 days. Net ear swelling was calculated by subtracting the thickness of the vehicle-treated ear from the thickness of the oxazolone-challenged ear. Adoptively transferred mice were sacrificed 3 days after the second application of oxazolone, and the analysis of the numbers of transplanted $CD4^+$ T cells was determined in the skin of the ears, the cervical draining lymph nodes, and the spleen. To analyze cells in the skin, the ears were removed from the mice and split into dorsal and ventral halves. The skin was placed in 2 ml of digestion buffer containing DNase I (0.1 mg/ml) and Liberase TL (0.2 mg/ml, Roche) diluted in 1% FBS in RPMI (GIBCO). After 1 hour of incubation at 37ºC, ears were placed into a 70-mm cell strainer (BD Biosciences) and mashed through the mesh. The strainers were washed with 2 ml of 1% FBS, 2 mM EDTA in PBS (GIBCO).

TIRF microscopy

J77 cells were co-transfected with plasmids encoding CD3ζ-EGFP and either dsRED or dsRED-Lamin-A. Transfected cells were sorted on a FACSAriaI flow cytometer, cultured for 1 day, and then plated onto 35-mm dishes (MatTek) coated with purified anti-CD3 antibody (T3b, 10 µg/ml). Images were acquired for 10 min at 0.35-s intervals on a Leica AM TIRFM MC unit

mounted on a Leica DMI6000B microscope fitted with a 100×/1.46 oil immersion objective, with 1.6× magnification and ~90-nm depth penetration. Images were analyzed with Imaris software (Bitplane) with a Brownian motion algorithm.

Statistical analysis

All statistical analyses were performed with Prism GraphPad or Microsoft Office Excel. Unless otherwise stated, statistical significance was calculated by two-tailed Student's t-test. When specified, one-way ANOVA or two-way ANOVA with Bonferroni's post-hoc multiple comparison test was used. Significance of differences was calculated as follows: $*P < 0.05$, $**P < 0.01$, and $***P < 0.001$.

Supplementary Materials

Fig. S1. Schemes of the protocols used to culture human PBLs and mouse splenocytes to generate human T lymphoblasts, human DCs, and mouse T lymphoblasts.
Fig. S2. Analysis of lamin-A/C and lamin-B1 in immune cells.
Fig. S3. $CD4^+$ T cells migrate to lymph nodes and have lamin-A/C in the hapten-induced contact hypersensitivity model.
Fig. S4. J77 cells stably expressing GFP-lamin-A display enhanced T cell activation.
Fig. S5. Lamin-A facilitates the interactions between J77 cells and APCs and modulates CD3 movement and clustering at the immunological synapse.
Fig. S6. Quantification of the numbers of $CD45.1^+$ and $CD45.2^+$ $CD4^+$ T cells in the blood of donor, recipient, and chimeric mice.
Movie S1. A-type lamins regulate several steps in the interaction between T cells and APCs.
Movie S2. Lamin-A regulates the movement of TCR-CD3 complexes in the plasma membrane.

References and Notes

1. V. Andrés, J. M. González, Role of A-type lamins in signaling, transcription, and chromatin organization. *J Cell Biol* **187**, 945-957 (2009).
2. J. L. Broers, F. C. Ramaekers, G. Bonne, R. B. Yaou, C. J. Hutchison, Nuclear lamins: laminopathies and their role in premature ageing. *Physiol Rev* **86**, 967-1008 (2006).
3. F. Houben, C. H. Willems, I. L. Declercq, K. Hochstenbach, M. A. Kamps, L. H. Snoeckx, F. C. Ramaekers, J. L. Broers, Disturbed nuclear orientation and cellular migration in A-type lamin deficient cells. *Biochim Biophys Acta* **1793**, 312-324 (2009).

4. D. A. Starr, H. N. Fridolfsson, Interactions between nuclei and the cytoskeleton are mediated by SUN-KASH nuclear-envelope bridges. *Annu Rev Cell Dev Biol* **26**, 421-444 (2010).
5. B. Burke, C. L. Stewart, The nuclear lamins: flexibility in function. *Nat Rev Mol Cell Biol* **14**, 13-24 (2012).
6. R. A. Rober, H. Sauter, K. Weber, M. Osborn, Cells of the cellular immune and hemopoietic system of the mouse lack lamins A/C: distinction versus other somatic cells. *J Cell Sci* **95 (Pt 4)**, 587-598 (1990).
7. M. Paulin-Levasseur, A. Scherbarth, U. Traub, P. Traub, Lack of lamins A and C in mammalian hemopoietic cell lines devoid of intermediate filament proteins. *Eur J Cell Biol* **47**, 121-131 (1988).
8. M. N. Guilly, A. Bensussan, J. F. Bourge, M. Bornens, J. C. Courvalin, A human T lymphoblastic cell line lacks lamins A and C. *EMBO J* **6**, 3795-3799 (1987).
9. M. P. Jansen, B. M. Machiels, A. H. Hopman, J. L. Broers, F. J. Bot, J. W. Arends, F. C. Ramaekers, H. C. Schouten, Comparison of A and B-type lamin expression in reactive lymph nodes and nodular sclerosing Hodgkin's disease. *Histopathology* **31**, 304-312 (1997).
10. M. N. Guilly, J. P. Kolb, F. Gosti, F. Godeau, J. C. Courvalin, Lamins A and C are not expressed at early stages of human lymphocyte differentiation. *Exp Cell Res* **189**, 145-147 (1990).
11. T. Bladon, K. Brasch, D. L. Brown, G. Setterfield, Changes in structure and protein composition of bovine lymphocyte nuclear matrix during concanavalin-A-induced mitogenesis. *Biochem Cell Biol* **66**, 40-53 (1988).
12. B. Stadelmann, E. Khandjian, A. Hirt, A. Luthy, R. Weil, H. P. Wagner, Repression of nuclear lamin A and C gene expression in human acute lymphoblastic leukemia and non-Hodgkin's lymphoma cells. *Leuk Res* **14**, 815-821 (1990).
13. C. B. Costa, J. Casalta-Lopes, C. Andrade, D. Moreira, A. Oliveira, A. C. Goncalves, V. Alves, T. Silva, M. Dourado, J. M. Nascimento-Costa, A. B. Sarmento-Ribeiro, Farnesyltransferase inhibitors: molecular evidence of therapeutic efficacy in acute lymphoblastic leukemia through cyclin D1 inhibition. *Anticancer Res* **32**, 831-838 (2012).
14. L. A. Wheeler, R. Trifonova, V. Vrbanac, E. Basar, S. McKernan, Z. Xu, E. Seung, M. Deruaz, T. Dudek, J. I. Einarsson, L. Yang, T. M. Allen, A. D. Luster, A. M. Tager, D. M. Dykxhoorn, J. Lieberman, Inhibition of HIV transmission in human cervicovaginal explants and humanized mice using CD4 aptamer-siRNA chimeras. *J Clin Invest* **121**, 2401-2412 (2011).
15. J. S. Hale, R. L. Frock, S. A. Mamman, P. J. Fink, B. K. Kennedy, Cell-extrinsic defective lymphocyte development in Lmna(-/-) mice. *PLoS One* **5**, e10127 (2010).
16. C. R. Monks, B. A. Freiberg, H. Kupfer, N. Sciaky, A. Kupfer, Three-dimensional segregation of supramolecular activation clusters in T cells. *Nature* **395**, 82-86 (1998).
17. M. L. Dustin, M. W. Olszowy, A. D. Holdorf, J. Li, S. Bromley, N. Desai, P. Widder, F. Rosenberger, P. A. van der Merwe, P. M. Allen, A. S. Shaw, A novel

adaptor protein orchestrates receptor patterning and cytoskeletal polarity in T-cell contacts. *Cell* **94**, 667-677 (1998).
18. C. Wulfing, M. M. Davis, A receptor/cytoskeletal movement triggered by costimulation during T cell activation. *Science* **282**, 2266-2269 (1998).
19. A. Grakoui, S. K. Bromley, C. Sumen, M. M. Davis, A. S. Shaw, P. M. Allen, M. L. Dustin, The immunological synapse: a molecular machine controlling T cell activation. *Science* **285**, 221-227 (1999).
20. D. R. Fooksman, S. Vardhana, G. Vasiliver-Shamis, J. Liese, D. A. Blair, J. Waite, C. Sacristan, G. D. Victora, A. Zanin-Zhorov, M. L. Dustin, Functional anatomy of T cell activation and synapse formation. *Annu Rev Immunol* **28**, 79-105 (2010).
21. D. D. Billadeau, J. C. Nolz, T. S. Gomez, Regulation of T-cell activation by the cytoskeleton. *Nat Rev Immunol* **7**, 131-143 (2007).
22. M. Vicente-Manzanares, F. Sánchez-Madrid, Role of the cytoskeleton during leukocyte responses. *Nat Rev Immunol* **4**, 110-122 (2004).
23. P. Bousso, E. Robey, Dynamics of CD8+ T cell priming by dendritic cells in intact lymph nodes. *Nat Immunol* **4**, 579-585 (2003).
24. T. R. Mempel, S. E. Henrickson, U. H. Von Andrian, T-cell priming by dendritic cells in lymph nodes occurs in three distinct phases. *Nature* **427**, 154-159 (2004).
25. M. F. Krummel, M. M. Davis, Dynamics of the immunological synapse: finding, establishing and solidifying a connection. *Curr Opin Immunol* **14**, 66-74 (2002).
26. S. Stoll, J. Delon, T. M. Brotz, R. N. Germain, Dynamic imaging of T cell-dendritic cell interactions in lymph nodes. *Science* **296**, 1873-1876 (2002).
27. T. Honda, G. Egawa, S. Grabbe, K. Kabashima, Update of immune events in the murine contact hypersensitivity model: toward the understanding of allergic contact dermatitis. *J Invest Dermatol* **133**, 303-315 (2013).
28. H. W. Murray, J. D. Berman, C. R. Davies, N. G. Saravia, Advances in leishmaniasis. *Lancet* **366**, 1561-1577 (2005).
29. V. Rocha-Perugini, M. Zamai, J. M. Gonzalez-Granado, O. Barreiro, E. Tejera, M. Yanez-Mo, V. R. Caiolfa, F. Sanchez-Madrid, CD81 controls sustained T cell activation signaling and defines the maturation stages of cognate immunological synapses. *Mol Cell Biol* **33**, 3644-3658 (2013).
30. A. D. Douglass, R. D. Vale, Single-molecule microscopy reveals plasma membrane microdomains created by protein-protein networks that exclude or trap signaling molecules in T cells. *Cell* **121**, 937-950 (2005).
31. N. B. Martin-Cofreces, J. Robles-Valero, J. R. Cabrero, M. Mittelbrunn, M. Gordon-Alonso, C. H. Sung, B. Alarcon, J. Vazquez, F. Sanchez-Madrid, MTOC translocation modulates IS formation and controls sustained T cell signaling. *J Cell Biol* **182**, 951-962 (2008).
32. M. L. Lombardi, D. E. Jaalouk, C. M. Shanahan, B. Burke, K. J. Roux, J. Lammerding, The interaction between nesprins and sun proteins at the nuclear envelope is critical for force transmission between the nucleus and cytoskeleton. *J Biol Chem* **286**, 26743-26753 (2011).

33. F. Haque, D. Mazzeo, J. T. Patel, D. T. Smallwood, J. A. Ellis, C. M. Shanahan, S. Shackleton, Mammalian SUN protein interaction networks at the inner nuclear membrane and their role in laminopathy disease processes. *J Biol Chem* **285**, 3487-3498 (2010).
34. F. Haque, D. J. Lloyd, D. T. Smallwood, C. L. Dent, C. M. Shanahan, A. M. Fry, R. C. Trembath, S. Shackleton, SUN1 interacts with nuclear lamin A and cytoplasmic nesprins to provide a physical connection between the nuclear lamina and the cytoskeleton. *Mol Cell Biol* **26**, 3738-3751 (2006).
35. R. A. Rober, K. Weber, M. Osborn, Differential timing of nuclear lamin A/C expression in the various organs of the mouse embryo and the young animal: a developmental study. *Development* **105**, 365-378 (1989).
36. J. L. Broers, B. M. Machiels, H. J. Kuijpers, F. Smedts, R. van den Kieboom, Y. Raymond, F. C. Ramaekers, A- and B-type lamins are differentially expressed in normal human tissues. *Histochem Cell Biol* **107**, 505-517 (1997).
37. F. Lin, H. J. Worman, Expression of nuclear lamins in human tissues and cancer cell lines and transcription from the promoters of the lamin A/C and B1 genes. *Exp Cell Res* **236**, 378-384 (1997).
38. C. J. Hutchison, H. J. Worman, A-type lamins: guardians of the soma? *Nat Cell Biol* **6**, 1062-1067 (2004).
39. R. Agrelo, F. Setien, J. Espada, M. J. Artiga, M. Rodriguez, A. Perez-Rosado, A. Sanchez-Aguilera, M. F. Fraga, M. A. Piris, M. Esteller, Inactivation of the lamin A/C gene by CpG island promoter hypermethylation in hematologic malignancies, and its association with poor survival in nodal diffuse large B-cell lymphoma. *J Clin Oncol* **23**, 3940-3947 (2005).
40. G. Lattanzi, M. Columbaro, E. Mattioli, V. Cenni, D. Camozzi, M. Wehnert, S. Santi, M. Riccio, R. Del Coco, N. M. Maraldi, S. Squarzoni, R. Foisner, C. Capanni, Pre-Lamin A processing is linked to heterochromatin organization. *J Cell Biochem* **102**, 1149-1159 (2007).
41. P. Gonnord, C. M. Blouin, C. Lamaze, Membrane trafficking and signaling: two sides of the same coin. *Semin Cell Dev Biol* **23**, 154-164 (2012).
42. Y. Kaizuka, A. D. Douglass, R. Varma, M. L. Dustin, R. D. Vale, Mechanisms for segregating T cell receptor and adhesion molecules during immunological synapse formation in Jurkat T cells. *Proc Natl Acad Sci U S A* **104**, 20296-20301 (2007).
43. J. Yi, X. S. Wu, T. Crites, J. A. Hammer, 3rd, Actin retrograde flow and actomyosin II arc contraction drive receptor cluster dynamics at the immunological synapse in Jurkat T cells. *Mol Biol Cell* **23**, 834-852 (2012).
44. T. Ilani, G. Vasiliver-Shamis, S. Vardhana, A. Bretscher, M. L. Dustin, T cell antigen receptor signaling and immunological synapse stability require myosin IIA. *Nat Immunol* **10**, 531-539 (2009).
45. C. A. Wilson, M. A. Tsuchida, G. M. Allen, E. L. Barnhart, K. T. Applegate, P. T. Yam, L. Ji, K. Keren, G. Danuser, J. A. Theriot, Myosin II contributes to cell-scale actin network treadmilling through network disassembly. *Nature* **465**, 373-377 (2010).

46. Y. Yu, N. C. Fay, A. A. Smoligovets, H. J. Wu, J. T. Groves, Myosin IIA modulates T cell receptor transport and CasL phosphorylation during early immunological synapse formation. *PLoS One* **7**, e30704 (2012).
47. K. H. Lee, A. D. Holdorf, M. L. Dustin, A. C. Chan, P. M. Allen, A. S. Shaw, T cell receptor signaling precedes immunological synapse formation. *Science* **295**, 1539-1542 (2002).
48. G. G. Garcia, R. A. Miller, Age-related defects in the cytoskeleton signaling pathways of CD4 T cells. *Ageing Res Rev* **10**, 26-34 (2011).
49. J. C. Stinchcombe, E. Majorovits, G. Bossi, S. Fuller, G. M. Griffiths, Centrosome polarization delivers secretory granules to the immunological synapse. *Nature* **443**, 462-465 (2006).
50. M. Mittelbrunn, C. Gutierrez-Vazquez, C. Villarroya-Beltri, S. Gonzalez, F. Sanchez-Cabo, M. A. Gonzalez, A. Bernad, F. Sanchez-Madrid, Unidirectional transfer of microRNA-loaded exosomes from T cells to antigen-presenting cells. *Nat Commun* **2**, 282 (2011).
51. E. J. Quann, E. Merino, T. Furuta, M. Huse, Localized diacylglycerol drives the polarization of the microtubule-organizing center in T cells. *Nat Immunol* **10**, 627-635 (2009).
52. A. Babich, S. Li, R. S. O'Connor, M. C. Milone, B. D. Freedman, J. K. Burkhardt, F-actin polymerization and retrograde flow drive sustained PLCgamma1 signaling during T cell activation. *J Cell Biol* **197**, 775-787 (2012).
53. V. C. Foletta, D. H. Segal, D. R. Cohen, Transcriptional regulation in the immune system: all roads lead to AP-1. *J Leukoc Biol* **63**, 139-152 (1998).
54. M. C. Castellanos, C. Munoz, M. C. Montoya, E. Lara-Pezzi, M. Lopez-Cabrera, M. O. de Landazuri, Expression of the leukocyte early activation antigen CD69 is regulated by the transcription factor AP-1. *J Immunol* **159**, 5463-5473 (1997).
55. D. D'Ambrosio, D. A. Cantrell, L. Frati, A. Santoni, R. Testi, Involvement of p21ras activation in T cell CD69 expression. *Eur J Immunol* **24**, 616-620 (1994).
56. P. Fernandez-Riejos, R. Goberna, V. Sanchez-Margalet, Leptin promotes cell survival and activates Jurkat T lymphocytes by stimulation of mitogen-activated protein kinase. *Clin Exp Immunol* **151**, 505-518 (2008).
57. R. Houben, H. Voigt, C. Noelke, V. Hofmeister, J. C. Becker, D. Schrama, MAPK-independent impairment of T-cell responses by the multikinase inhibitor sorafenib. *Mol Cancer Ther* **8**, 433-440 (2009).
58. X. Wang, J. Hao, D. L. Metzger, Z. Ao, L. Chen, D. Ou, C. B. Verchere, A. Mui, G. L. Warnock, B7-H4 Treatment of T Cells Inhibits ERK, JNK, p38, and AKT Activation. *PLoS One* **7**, e28232 (2012).
59. J. M. Gonzalez, A. Navarro-Puche, B. Casar, P. Crespo, V. Andres, Fast regulation of AP-1 activity through interaction of lamin A/C, ERK1/2, and c-Fos at the nuclear envelope. *J Cell Biol* **183**, 653-666 (2008).
60. K. Wilhelmsen, S. H. Litjens, I. Kuikman, N. Tshimbalanga, H. Janssen, I. van den Bout, K. Raymond, A. Sonnenberg, Nesprin-3, a novel outer nuclear membrane protein, associates with the cytoskeletal linker protein plectin. *J Cell Biol* **171**, 799-810 (2005).

61. D. Geerts, L. Fontao, M. G. Nievers, R. Q. Schaapveld, P. E. Purkis, G. N. Wheeler, E. B. Lane, I. M. Leigh, A. Sonnenberg, Binding of integrin alpha6beta4 to plectin prevents plectin association with F-actin but does not interfere with intermediate filament binding. *J Cell Biol* **147**, 417-434 (1999).
62. Y. Y. Zhen, T. Libotte, M. Munck, A. A. Noegel, E. Korenbaum, NUANCE, a giant protein connecting the nucleus and actin cytoskeleton. *J Cell Sci* **115**, 3207-3222 (2002).
63. N. Wang, J. D. Tytell, D. E. Ingber, Mechanotransduction at a distance: mechanically coupling the extracellular matrix with the nucleus. *Nat Rev Mol Cell Biol* **10**, 75-82 (2009).
64. J. Herter, A. Zarbock, Integrin Regulation during Leukocyte Recruitment. *J Immunol* **190**, 4451-4457 (2013).
65. E. Judokusumo, E. Tabdanov, S. Kumari, M. L. Dustin, L. C. Kam, Mechanosensing in T lymphocyte activation. *Biophys J* **102**, L5-7 (2012).
66. N. Martinez-Martin, E. Fernandez-Arenas, S. Cemerski, P. Delgado, M. Turner, J. Heuser, D. J. Irvine, B. Huang, X. R. Bustelo, A. Shaw, B. Alarcon, T cell receptor internalization from the immunological synapse is mediated by TC21 and RhoG GTPase-dependent phagocytosis. *Immunity* **35**, 208-222 (2011).
67. A. Busch, T. Kiel, W. M. Heupel, M. Wehnert, S. Hubner, Nuclear protein import is reduced in cells expressing nuclear envelopathy-causing lamin A mutants. *Exp Cell Res* **315**, 2373-2385 (2009).
68. J. L. Broers, B. M. Machiels, G. J. van Eys, H. J. Kuijpers, E. M. Manders, R. van Driel, F. C. Ramaekers, Dynamics of the nuclear lamina as monitored by GFP-tagged A-type lamins. *J Cell Sci* **112 (Pt 20)**, 3463-3475 (1999).
69. S. Ibiza, V. M. Víctor, I. Boscá, A. Ortega, A. Urzainqui, J. E. O'Connor, F. Sánchez-Madrid, J. V. Esplugues, J. M. Serrador, Endothelial nitric oxide synthase regulates T cell receptor signaling at the immunological synapse. *Immunity* **24**, 753-765 (2006).
70. J. Harriague, G. Bismuth, Imaging antigen-induced PI3K activation in T cells. *Nat Immunol* **3**, 1090-1096 (2002).
71. T. Sullivan, D. Escalante-Alcalde, H. Bhatt, M. Anver, N. Bhat, K. Nagashima, C. L. Stewart, B. Burke, Loss of A-type lamin expression compromises nuclear envelope integrity leading to muscular dystrophy. *J Cell Biol* **147**, 913-920 (1999).
72. H. Spits, G. Keizer, J. Borst, C. Terhorst, A. Hekman, J. E. de Vries, Characterization of monoclonal antibodies against cell surface molecules associated with cytotoxic activity of natural and activated killer cells and cloned CTL lines. *Hybridoma* **2**, 423-437 (1983).
73. M. Cebrian, E. Yague, M. Rincon, M. Lopez-Botet, M. O. de Landazuri, F. Sanchez-Madrid, Triggering of T cell proliferation through AIM, an activation inducer molecule expressed on activated human lymphocytes. *J Exp Med* **168**, 1621-1637 (1988).
74. A. C. Carrera, F. Sanchez-Madrid, M. Lopez-Botet, C. Bernabeu, M. O. De Landazuri, Involvement of the CD4 molecule in a post-activation event on T cell proliferation. *Eur J Immunol* **17**, 179-186 (1987).

75. C. Calabia-Linares, J. Robles-Valero, H. de la Fuente, M. Pérez-Martínez, N. Martín-Cofreces, M. Alfonso-Pérez, C. Gutiérrez-Vázquez, M. Mittelbrunn, S. Ibiza, F. R. Urbano-Olmos, C. Aguado-Ballano, C. O. Sánchez-Sorzano, F. Sánchez-Madrid, E. Veiga, Endosomal clathrin drives actin accumulation at the immunological synapse. *J Cell Sci* **124**, 820-830 (2011).

Acknowledgments: We thank J. Mateos, V. Zorita, A. del Monte, S. di Costanzo, V. Fanjul, R. Fontanella, and L. Cirillo for help with some experiments and animal care; S. Bartlett for editing the manuscript; M. J. Andrés-Manzano for figure preparation; B. Dorado for critical reading of the manuscript; and X. Bustelo, J. Lammerding, and S. Shackleton for providing reagents. **Funding:** Work in the authors' laboratories is supported by the Ministerio de Economía y Competitividad (MINECO) (SAF2011-25834 and SAF2010-16044); Comunidad de Madrid (INDISNET-S2011/BMD-2332); Instituto de Salud Carlos III (ISCIII) (RD12/0042/0028, RD12/0042/0056, and CP11/00145); The Progeria Research Foundation (Innovator Award PRF 2012-42); and the European Commission (ERC-2011AdG 294340-GENTRIS, Grant No 317916-Liphos). C.L.-O. is an Investigator of the Botín Foundation. J.M.G.-G. received salary support from the Sara Borrell and Miguel Servet (CP11/00145) ISCIII programs. C.S.-R. received salary support from the Fundación Mario Losantos del Campo and Fundación Ferrer para la Investigación. The Instituto Universitario de Oncología is supported by Obra Social Cajastur, and the CNIC is supported by the MINECO and Pro-CNIC Foundation. **Author contributions:** J.M.G.G., C.S.-R., V.R.P., L.T.M., D.C., G.M., and M.B.B. performed the experiments; F.G.O., J.M.P.F., and C.L.-O. contributed new reagents; J.M.G.-G., F.S.M., and V.A. supervised the project, designed experiments, interpreted data, and wrote the paper; and V.R.P., C.L.-O., C.S.-R., and L.T.-M. revised the manuscript. **Competing interests:** The authors declare that they have no competing interests.

Fig. 1. **A-type lamins are increased in abundance upon T cell activation.** (**A**) Human $CD4^+$ PBLs and mouse splenocytes were incubated with antibodies specific for lamin-A/C (red) and CD4 (green) and then were analyzed by confocal microscopy. A single confocal plane is shown. (**B**) Human PBLs were incubated with antibodies specific for CD4 and lamin-A/C and then were analyzed by flow cytometry. Cells stained with isotype control antibody were used as negative control (gray). The graph shows quantification of the percentage of $CD4^+$ T cells that have lamin-A/C. Data are means ± SEM from five donors. (**C** to **E**) Time course of the increase in lamin-A/C abundance in $CD4^+$ PBLs and T lymphoblasts. (C) SEE-treated human PBLs were analyzed by flow cytometry and Western blotting. Top: Representative flow cytometry

histograms. Middle: Quantification of flow cytometry histograms. Bottom: Representative Western blot. (D) Phytohemagglutinin (PHA)-treated human T lymphoblasts were analyzed by flow cytometry and Western blotting. Top: Representative flow cytometry histograms. Bottom: Representative Western blot. (E) T lymphoblasts from OTII transgenic mice were stimulated with OVA-loaded DCs and analyzed by flow cytometry. Top: Representative flow cytometry histograms. Bottom: Quantification of flow cytometry histograms. Histograms of cells stained with isotype control antibody are filled in gray. Graphs show the fold-increase in the abundance in lamin-A/C with respect to the quantity at day 0 before stimulation. Data are means ± SEM from three to five donors.

Fig. 2. Loss of A-type lamins impairs T cell activation in vitro and in vivo. (**A**) Wild-type (WT) and *Lmna*$^{-/-}$ splenocytes were unstimulated or stimulated for 2 hours with anti-CD3 and anti-CD28 antibodies, PMA and ionomycin (PMA+Iono), or concanavalin A and then were analyzed by quantitative PCR to determine their relative amounts of *Cd25* mRNA. The graphs show the amount of mRNA relative to that in wild-type cells without stimulation and are means ± SEM from three independent experiments, analyzed by one-way ANOVA. (**B**) CD4^{+} splenocytes isolated from pools of two to nine *Lmna*$^{-/-}$) or WT mice were stimulated with anti-CD3 and anti-CD28 antibodies for 24 hours and then were analyzed by flow cytometry to determine the cell-surface abundances of CD69 and CD25. The graphs show the percentages of CD25^{+} or CD69^{+} cells relative to those among wild-type cells and are means ± SEM from three independent experiments. Representative histograms of CD25 or CD69 staining are shown. (**C**) CD4^{+} splenocytes isolated from pools of three to nine OTII *Lmna*$^{-/-}$ or OTII WT mice were stimulated with either non-loaded or OVA peptide-loaded DCs for 24 hours, and then were

analyzed by flow cytometry to determine cell-surface CD25 abundance. The graph shows the percentages of $CD25^+$ cells relative to those among wild-type cells and are means ± SEM from three independent experiments. Representative histograms of CD25 staining are shown. (**D**) Measurement of the contact hypersensitivity response to oxalazone in the ears of lethally-irradiated WT recipient mice that were reconstituted with bone marrow cells from WT or *Lmna*$^{-/-}$ mice. Data represent the extent of ear swelling in 10 mice of each group and are means ± SEM, analyzed by two-way ANOVA. (**E**) $CD4^+$ T-cells from $CD45.2^+$ WT and $CD45.2^+$ *Lmna*$^{-/-}$ mice were isolated and adoptively transferred into different groups of $CD45.1^+$ WT mice before the first application of oxazolone. Three days after the second application, the percentages of transferred $CD45.2^+CD4^+$ T cells relative to the recipient $CD45.1^+CD4^+$ T cells in the ears were quantified by flow cytometry. Data are means ± SEM from six to seven mice. (**F**) $CD4^+$ T-cells from $CD45.2^+CD45.1^+$ WT and $CD45.2^+$ *Lmna*$^{-/-}$ mice were isolated, mixed at a 1:1 ratio, and adoptively transferred to $CD45.1^+$ WT mice before the application of oxazolone. Left histogram shows a representative experiment with the proportions of $CD45.2^+$ and $CD45.1^+CD45.2^+$ cells that were adoptively transferred. Three days after the second application of oxazolone, the percentages of $CD45.2^+$ *Lmna*$^{-/-}$ and $CD45.1^+CD45.2^+$ WT $CD4^+$ T cells relative to the total number of $CD4^+CD45.2^+$ T cells in the ears, draining lymph nodes, and spleens were quantified by flow cytometry, as shown in the representative histograms. Data are means ± SEM from eight mice.

Fig. 3. Lamin-A enhances the activation of human J77 cells. (**A**) J77 cells stably expressing GFP (J77-GFP) or GFP-Lamin-A (J77-GFP-Lamin-A) were incubated with either unloaded Raji cells or SEE-loaded Raji cells for the indicated times before being subjected to quantitative PCR

analysis to determine the relative amounts of *CD69* and *CD25* mRNAs. (**B**) J77-GFP or J77-GFP-Lamin-A cells were stimulated with either unloaded Raji cells or SEE-loaded Raji cells for 16 hours and then were analyzed by flow cytometry to determine the cell-surface abundance of CD69. Histograms show a representative experiment. The graph shows the percentages of $CD69^+$ cells in the indicated conditions relative to those among J77-GFP cells conjugated with unloaded Raji cells and are means ± SEM from three independent experiments, analyzed by one-way ANOVA. (**C**) J77-GFP or J77-GFP-Lamin-A cells were stimulated for 6, 18, or 24 hours with anti-CD3 and anti-CD28 antibodies and then were analyzed by flow cytometry to determine the cell-surface abundance of CD69. The histogram shows a representative experiment at 18 hours, and the graph shows fold changes in the percentage of $CD69^+$ cells at the indicated times relative to the percentage of J77-GFP cells that were $CD69^+$ after stimulation with anti-CD3 and anti-CD28 antibodies for 6 hours. Data are means ± SEM from three independent experiments and were analyzed by two-way ANOVA.

Fig. 4. Lamin-A modulates the dynamics of human J77 cell-Raji cell interactions. (**A**) J77-GFP or J77-GFP-Lamin-A cells were incubated with CMAC-labeled, unloaded or SEE-loaded Raji cells , incubated with an anti-α-tubulin antibody, and then analyzed by confocal microscopy. Representative images are of cell conjugates formed after 5 min. Raji cells are in red, whereas staining with the anti-α-tubulin antibody is in green. A single confocal plane is shown. Graph shows the percentages of cell conjugates at the indicated times. Data are means ± SEM of 300 to 500 conjugates from two independent experiments and were analyzed by two-way ANOVA. (**B** to **E**) J77-GFP cells (cyan and green) and J77-GFP-Lamin-A cells (red) were mixed in equal amounts and added onto SEE-loaded Raji cells (dark blue) that had been plated

onto PLL-coated coverslips. (B) Representative confocal video microscopy images of the conjugation of J77-GFP cells or J77-GFP-Lamin-A cells with SEE-loaded Raji cells at the indicated times. A single confocal plane is shown. (C) Percentages of cells that arrived at the focal plane by the indicated time frame. (D) Percentages of the indicated J77 cells that formed conjugates with Raji cells over time. Data are means ± SEM from thee independent experiments, and were analyzed by two-way ANOVA. (E) Duration of the interactions between the indicated J77 cells and Raji cells. Data are means ± SEM from three independent experiments.

Fig. 5. Lamin-A is required for optimal movement of TCR-CD3 complexes within the plasma membrane and TCR-dependent signaling. J77 cells were co-transfected with plasmids encoding CD3ζ-EGFP and either dsRED or dsRED-Lamin-A, sorted by flow cytometry on the basis of the detection of dsRED and GFP, plated onto anti-CD3 antibody-coated coverslips, and analyzed by TIRF microscopy at a penetration depth of ~90 nm. (**A**) Representative TIRF microscopy images of CD3ζ-EGFP at the indicated times. (**B** to **D**) The graphs show (B) the number of microclusters at each time point, (C) the area of the cSMAC at each time point, and (D) the duration of the tracks of each CD3 microcluster at the plasma membrane. Data are means ± SEM of 10 to 13 cells of each condition from three independent experiments. (**E**) J77-GFP and J77-GFP-lamin-A cells were allowed to form conjugates with SEE-loaded Raji cells for the indicated times before being lysed and analyzed by Western blotting to detect total and phosphorylated forms of Vav, ERK1/2, PLC-γ1, and myosin IIA. MW: Molecular weight marker. Representative blots are shown. Graphs show quantification of the ratios of phosphorylated to total proteins and are means ± SEM from three independent experiments. (**F**) J77-GFP or J77-GFP-lamin-A cells were allowed to form conjugates with unloaded (time 0) or

SEE-loaded Raji cells for the indicated times in the presence or absence of the MEK1/2 inhibitor U0126. Cells were then incubated with antibody against CD69 and analyzed by flow cytometry. Histograms show a representative experiment. Graph shows the fold-change in the cell-surface abundance of CD69 in the indicated cells relative to that in J77-GFP cells incubated with unloaded Raji cells. Data are means ± SEM from three independent experiments, and were analyzed by one-way ANOVA.

Fig. 6. A-type lamins promote MTOC translocation and F-actin polymerization in activated T cells. (**A**) J77-GFP and J77-GFP-lamin-A cells were allowed to form conjugates with CMAC-labeled, unloaded or SEE-loaded Raji cells (red) for the indicated times before they were stained with an anti-α-tubulin antibody and analyzed by confocal microscopy. Representative images are of cell conjugates at 5 min. Tubulin is in green, arrowheads point to the MTOC, and asterisks indicate Raji cells. A single confocal plane is shown. The graph shows quantification of the distance (in μm) between the MTOC and the J77 cell–Raji cell contact area at the indicated times after conjugate formation. Data are means ± SEM of at least 300 conjugates from three independent experiments and were analyzed by two-way ANOVA. (**B**) J77-GFP (white) and J77-GFP-lamin-A (black) cells were stimulated with coated anti-CD3 antibody and soluble anti-CD28 antibody, stained for phalloidin, and analyzed by flow cytometry. Data represent the fold change in the extent of F-actin polymerization relative to that in J77-GFP cells without antibodies at time zero. Data are means ± SEM from three independent experiments and were analyzed by two-way ANOVA. (**C**) J77-GFP and J77-GFP-lamin-A cells conjugated with SEE-loaded Raji cells were stained with phalloidin to detect F-actin and were analyzed by confocal microscopy. Representative projections of confocal stack images are

shown in which F-actin staining is depicted in pseudocolor intensity-coding format (maximum intensity is white), GFP is in green, and merged images depict GFP in green and F-actin staining in red. White asterisks indicate Raji cells. Right graph shows the amount of F-actin accumulation at the immunological synapse. Data are means ± SEM of 200 conjugates from three independent experiments. (**D**) Western blotting analysis of human T lymphoblasts transfected with control siRNA (siRNA-CTRL) or lamin-A/C-specific siRNA (siRNA-LMNA). (**E** and **F**) Human T lymphoblasts transfected with siRNA-CTRL or siRNA-LMNA were stimulated with (E) SEE-loaded Raji cells or (F) anti-CD3 and anti-CD28 antibodies for the indicated times, stained for F-actin, and then analyzed by flow cytometry. Data represent fold-changes in the amount of F-actin polymerization relative to that in (E) siRNA-CTRL-treated cells incubated with unloaded Raji B cells or (F) T lymphoblasts that were not stimulated with antibodies. Data are means ± SEM from three independent experiments and were analyzed by two-way ANOVA.

Fig. 7. The lamin-A–mediated increase in the extent of T cell activation requires a physical connection between the nucleus and the cytoskeleton through the LINC complex. (**A**) J77-GFP and J77-GFP-lamin-A cells expressing Cherry or a Cherry-tagged dominant negative form of the nesprin KASH domain (DN KASH) were conjugated for 16 hours with SEE-loaded Raji cells, incubated with antibody for CD69, and analyzed by flow cytometry. Histograms show a representative experiment. Right graph represents the fold increase in the percentage of $CD69^+$ cells with respect to the GFP^+ Cherry-expressing cells (first bar). (**B**) J77-GFP-lamin-A cells expressing DN KASH (black) or Cherry (white) were conjugated with SEE-loaded Raji cells for the indicated times, fixed, permeabilized, stained for F-actin, and then analyzed by flow cytometry. Data are the fold-change in F-actin content with respect to that in Cherry-expressing

cells in the absence of SEE-loaded Raji cells (0 min). Data are means ± SEM from three independent experiments and were analyzed by two-way ANOVA. (**C**) J77-GFP-lamin-A cells expressing Cherry (white) or Cherry and DN SUN (black) were incubated with SEE-loaded Raji cells for the indicated times, fixed, permeabilized, stained for F-actin, and then analyzed by flow cytometry. Data are the fold-change in F-actin content in the indicated cells relative to that in Cherry-expressing cells in the absence of SEE-loaded Raji cells (0 min). Data in (A) and (B) are means ± SEM from three independent experiments and were analyzed by two-way ANOVA.

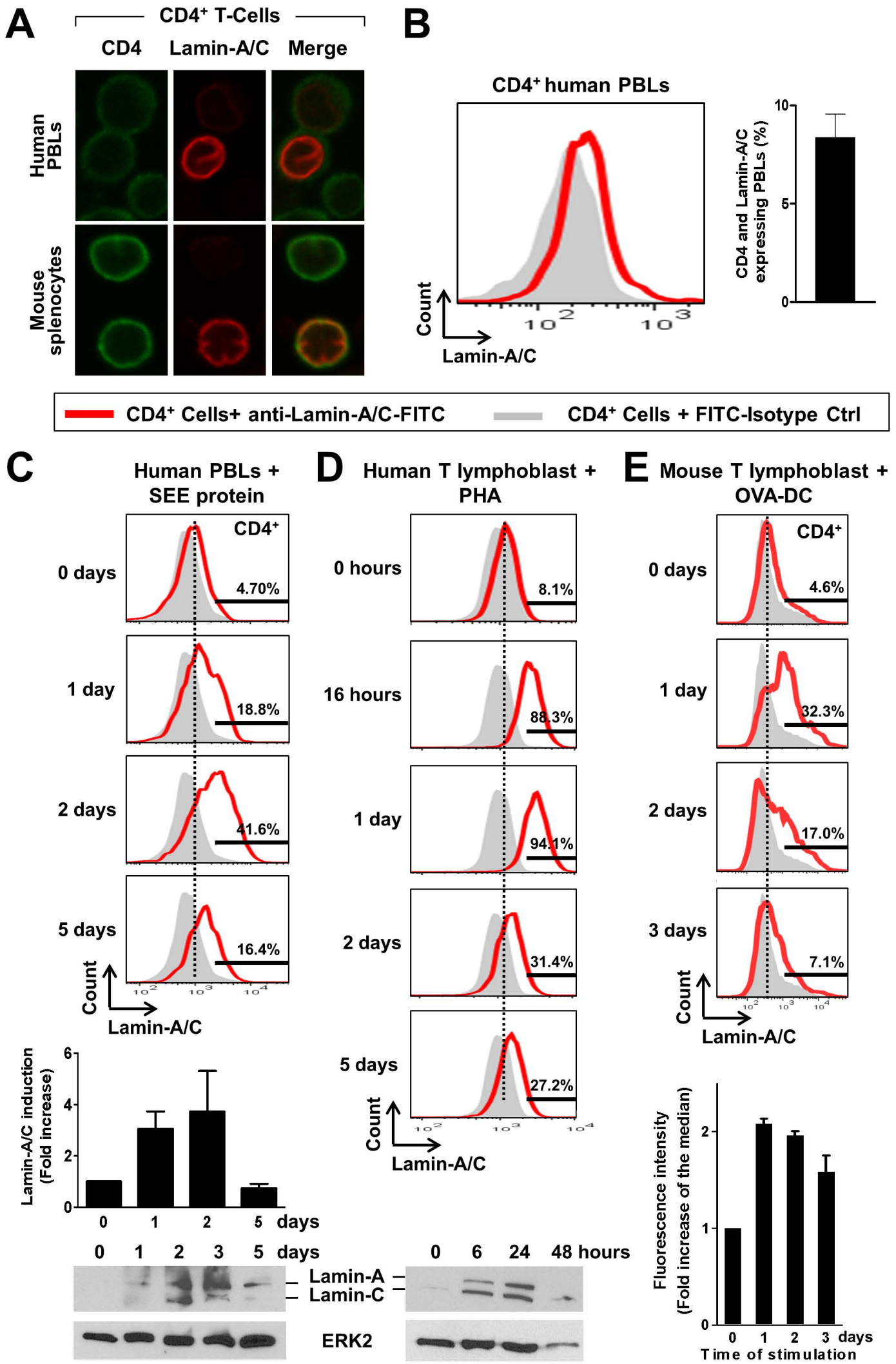
A
CD4+ T-Cells
CD4
Lamin-A/C
Merge
Human PBLs
Mouse splenocytes
B
CD4+ human PBLs
Count
Lamin-A/C
CD4 and Lamin-A/C expressing PBLs (%)
CD4+ Cells+ anti-Lamin-A/C-FITC
CD4+ Cells + FITC-Isotype Ctrl
C
Human PBLs + SEE protein
CD4+
0 days
4.70%
1 day
18.8%
2 days
41.6%
5 days
16.4%
Count
Lamin-A/C
Lamin-A/C induction (Fold increase)
0 1 2 5 days
D
Human T lymphoblast + PHA
0 hours
8.1%
16 hours
88.3%
1 day
94.1%
2 days
31.4%
5 days
27.2%
Count
Lamin-A/C
E
Mouse T lymphoblast + OVA-DC
CD4+
0 days
4.6%
1 day
32.3%
2 days
17.0%
3 days
7.1%
Count
Lamin-A/C
Fluorescence intensity (Fold increase of the median)
0 1 2 3 days
Time of stimulation
0 1 2 3 5 days
0 6 24 48 hours
Lamin-A
Lamin-C
ERK2

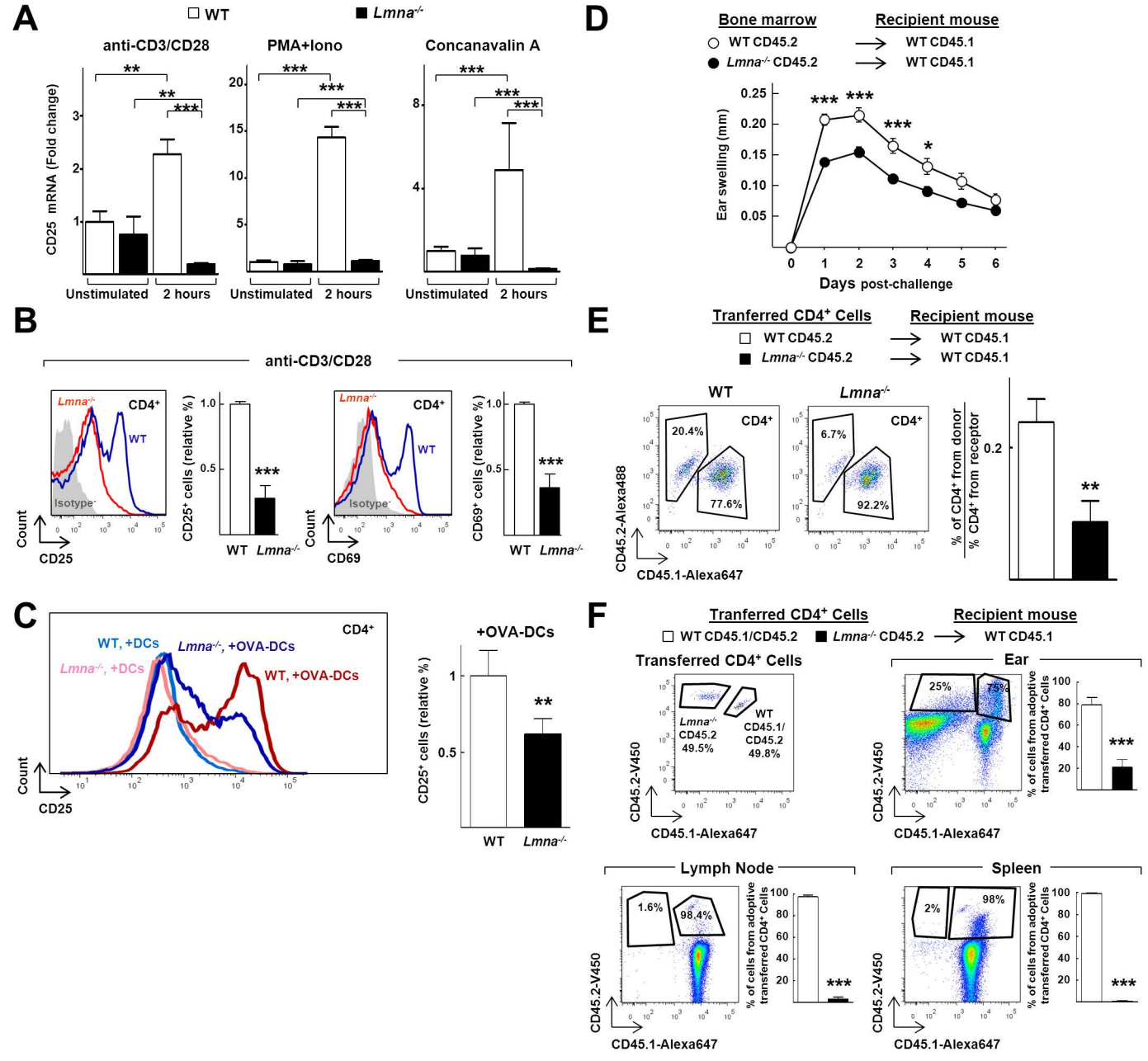
A
WT
Lmna-/-
anti-CD3/CD28
PMA+Iono
Concanavalin A
CD25 mRNA (Fold change)
Unstimulated
2 hours
B
anti-CD3/CD28
CD4+
Isotype
Count
CD25
CD69
CD25+ cells (relative %)
CD69+ cells (relative %)
C
WT, +DCs
Lmna-/-, +DCs
Lmna-/-, +OVA-DCs
WT, +OVA-DCs
+OVA-DCs
CD25+ cells (relative %)
D
Bone marrow
Recipient mouse
WT CD45.2
Lmna-/- CD45.2
WT CD45.1
Ear swelling (mm)
Days post-challenge
E
Tranferred CD4+ Cells
Recipient mouse
WT CD45.2
Lmna-/- CD45.2
WT CD45.1
20.4%
77.6%
6.7%
92.2%
CD45.2-Alexa488
CD45.1-Alexa647
% of CD4+ from donor
% CD4+ from receptor
F
Tranferred CD4+ Cells
Recipient mouse
WT CD45.1/CD45.2
Lmna-/- CD45.2
WT CD45.1
Transferred CD4+ Cells
Lmna-/- CD45.2 49.5%
WT CD45.1/ CD45.2 49.8%
Ear
25%
75%
Lymph Node
1.6%
98.4%
Spleen
2%
98%
CD45.2-V450
CD45.1-Alexa647
% of cells from adoptive transferred CD4+ Cells

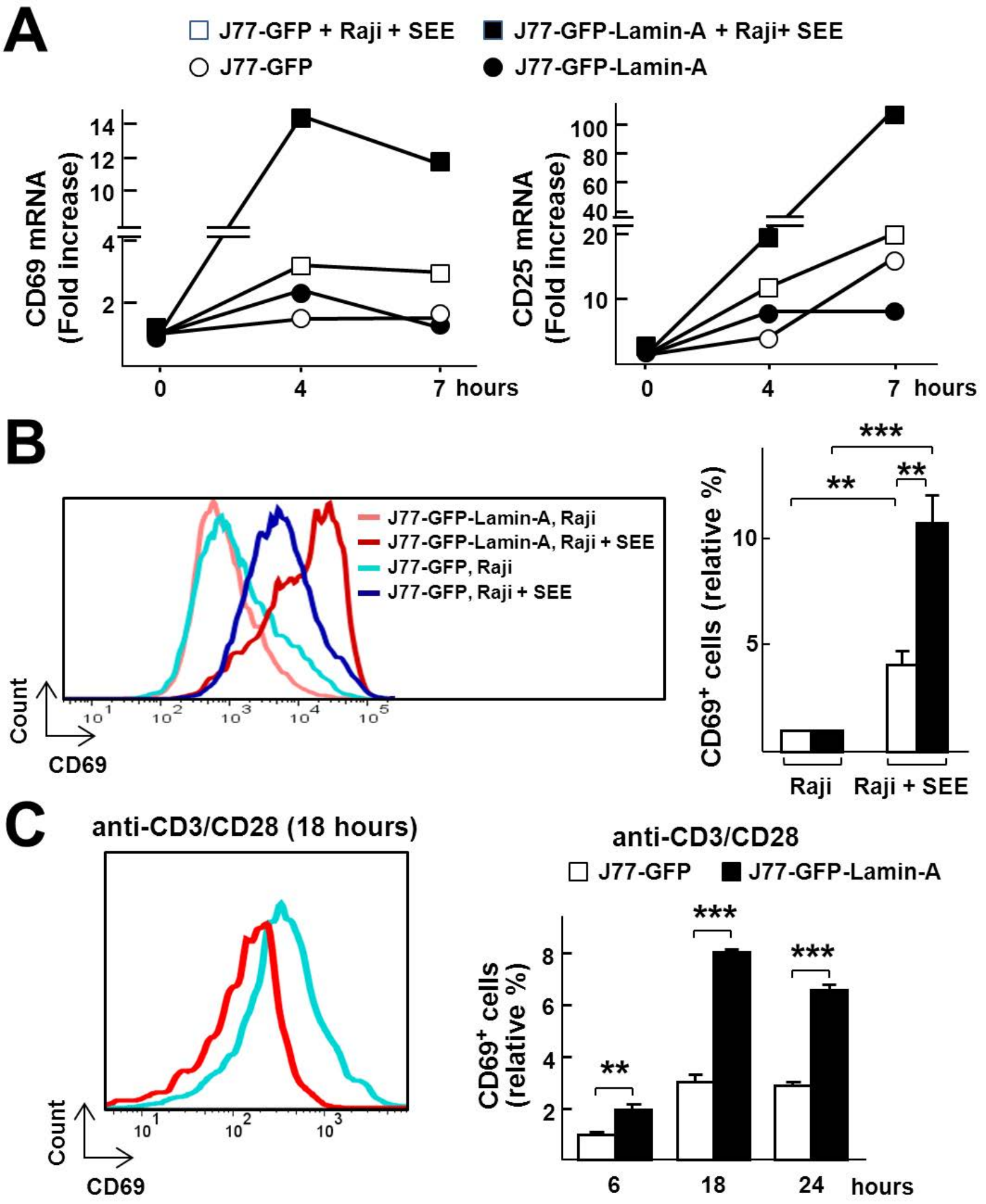
A
J77-GFP + Raji + SEE
J77-GFP-Lamin-A + Raji+ SEE
J77-GFP
J77-GFP-Lamin-A
CD69 mRNA (Fold increase)
14
12
10
4
2
0
4
7 hours
CD25 mRNA (Fold increase)
100
80
60
40
20
10
0
4
7 hours
B
J77-GFP-Lamin-A, Raji
J77-GFP-Lamin-A, Raji + SEE
J77-GFP, Raji
J77-GFP, Raji + SEE
Count
CD69
CD69+ cells (relative %)
***
**
**
10
5
Raji
Raji + SEE
C
anti-CD3/CD28 (18 hours)
Count
CD69
anti-CD3/CD28
J77-GFP
J77-GFP-Lamin-A
CD69+ cells (relative %)
***
***
**
8
6
4
2
6
18
24
hours

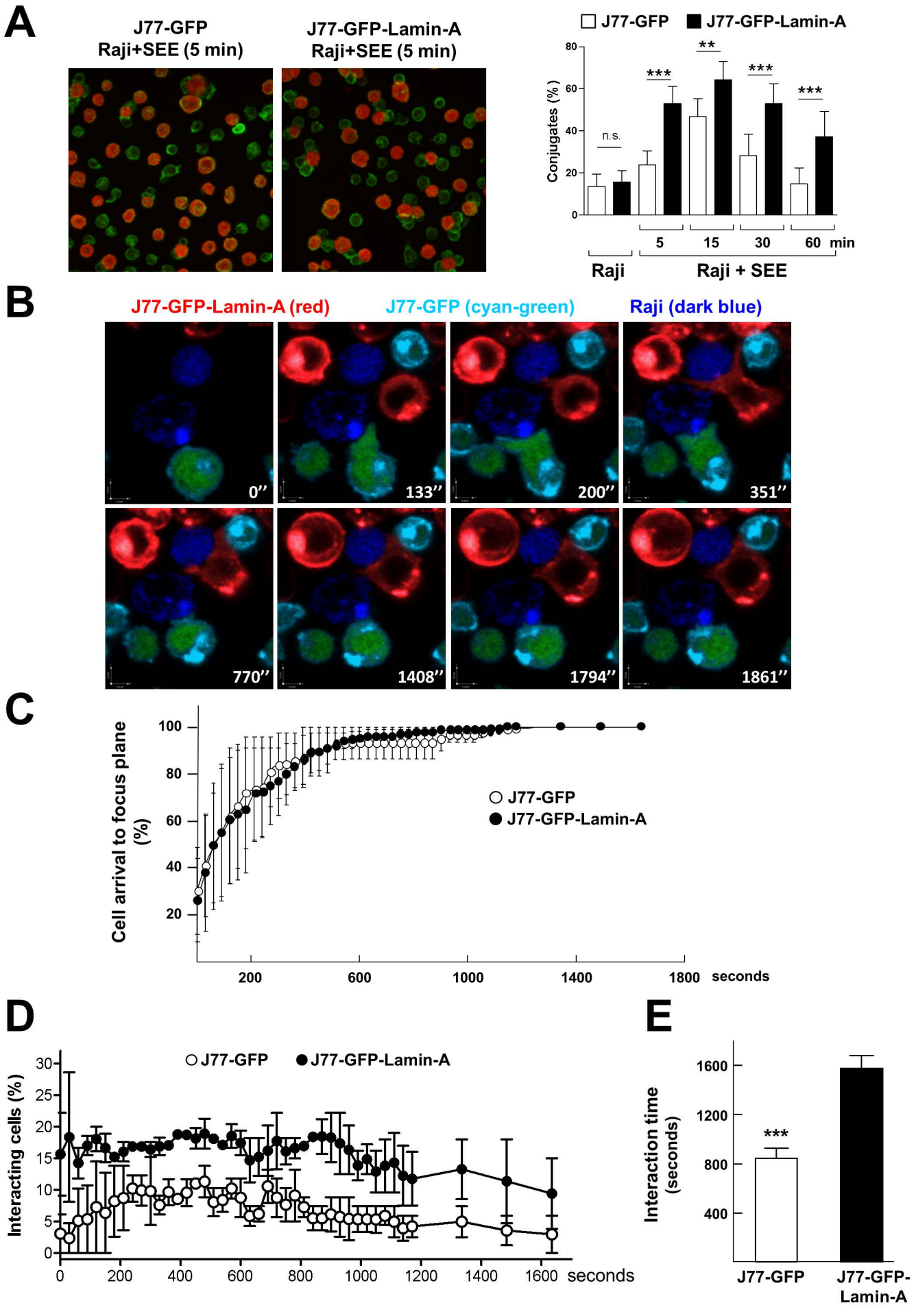
A
J77-GFP
Raji+SEE (5 min)
J77-GFP-Lamin-A
Raji+SEE (5 min)
J77-GFP
J77-GFP-Lamin-A
Conjugates (%)
n.s.
***
**
***
***
5
15
30
60 min
Raji
Raji + SEE
B
J77-GFP-Lamin-A (red)
J77-GFP (cyan-green)
Raji (dark blue)
0''
133''
200''
351''
770''
1408''
1794''
1861''
C
Cell arrival to focus plane (%)
J77-GFP
J77-GFP-Lamin-A
seconds
D
Interacting cells (%)
J77-GFP
J77-GFP-Lamin-A
seconds
E
Interaction time (seconds)
***
J77-GFP
J77-GFP-Lamin-A

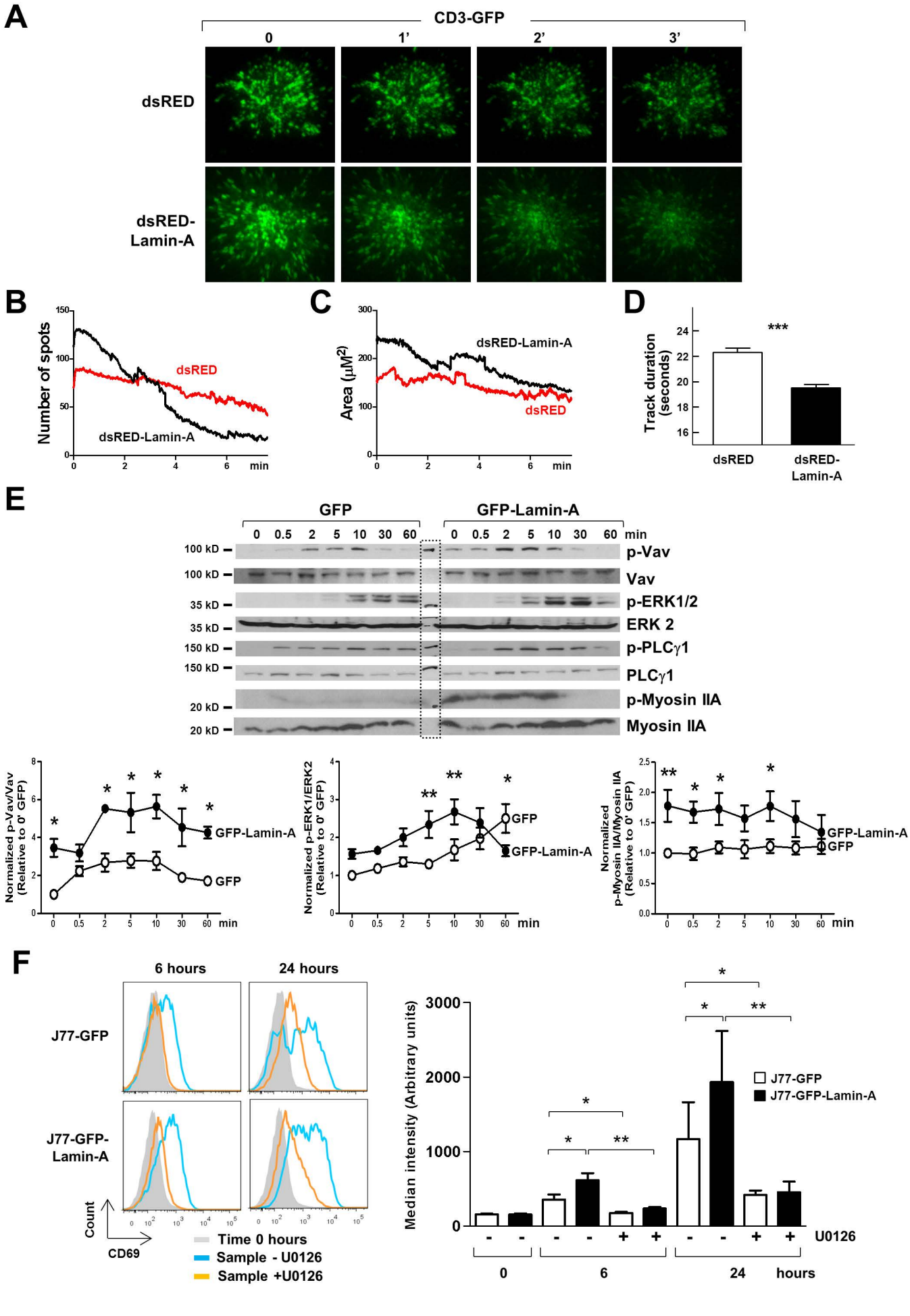
A
CD3-GFP
0
1'
2'
3'
dsRED
dsRED-Lamin-A
B
Number of spots
dsRED
dsRED-Lamin-A
min
C
Area (μM²)
dsRED-Lamin-A
dsRED
min
D
Track duration (seconds)
***
dsRED
dsRED-Lamin-A
E
GFP
GFP-Lamin-A
0 0.5 2 5 10 30 60 0 0.5 2 5 10 30 60 min
100 kD
p-Vav
100 kD
Vav
35 kD
p-ERK1/2
35 kD
ERK 2
150 kD
p-PLCγ1
150 kD
PLCγ1
20 kD
p-Myosin IIA
20 kD
Myosin IIA
Normalized p-Vav/Vav (Relative to 0' GFP)
GFP-Lamin-A
GFP
min
Normalized p-ERK1/ERK2 (Relative to 0' GFP)
GFP
GFP-Lamin-A
min
Normalized p-Myosin IIA/Myosin IIA (Relative to 0' GFP)
GFP-Lamin-A
GFP
min
F
6 hours
24 hours
J77-GFP
J77-GFP-Lamin-A
Count
CD69
Time 0 hours
Sample - U0126
Sample +U0126
Median intensity (Arbitrary units)
J77-GFP
J77-GFP-Lamin-A
U0126
0
6
24
hours

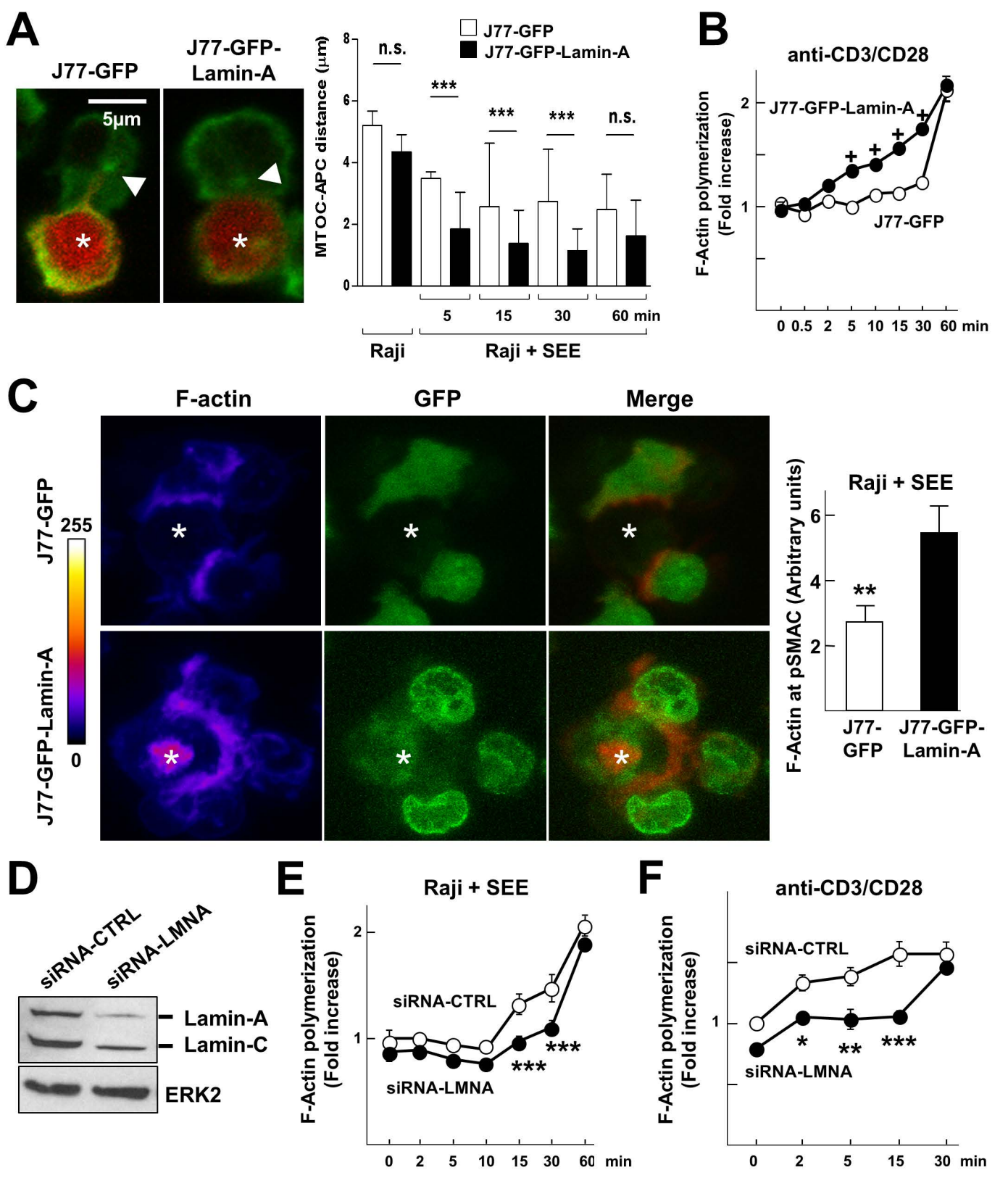
A
J77-GFP
J77-GFP-Lamin-A
5µm
J77-GFP
J77-GFP-Lamin-A
MTOC-APC distance (µm)
n.s.
***
***
***
n.s.
5
15
30
60 min
Raji
Raji + SEE
B
anti-CD3/CD28
J77-GFP-Lamin-A
J77-GFP
F-Actin polymerization (Fold increase)
0 0.5 2 5 10 15 30 60 min
C
F-actin
GFP
Merge
J77-GFP
J77-GFP-Lamin-A
255
0
Raji + SEE
F-Actin at pSMAC (Arbitrary units)
**
J77-GFP
J77-GFP-Lamin-A
D
siRNA-CTRL
siRNA-LMNA
Lamin-A
Lamin-C
ERK2
E
Raji + SEE
F-Actin polymerization (Fold increase)
siRNA-CTRL
siRNA-LMNA
***
***
0 2 5 10 15 30 60 min
F
anti-CD3/CD28
F-Actin polymerization (Fold increase)
siRNA-CTRL
siRNA-LMNA
*
**
***
0 2 5 15 30 min

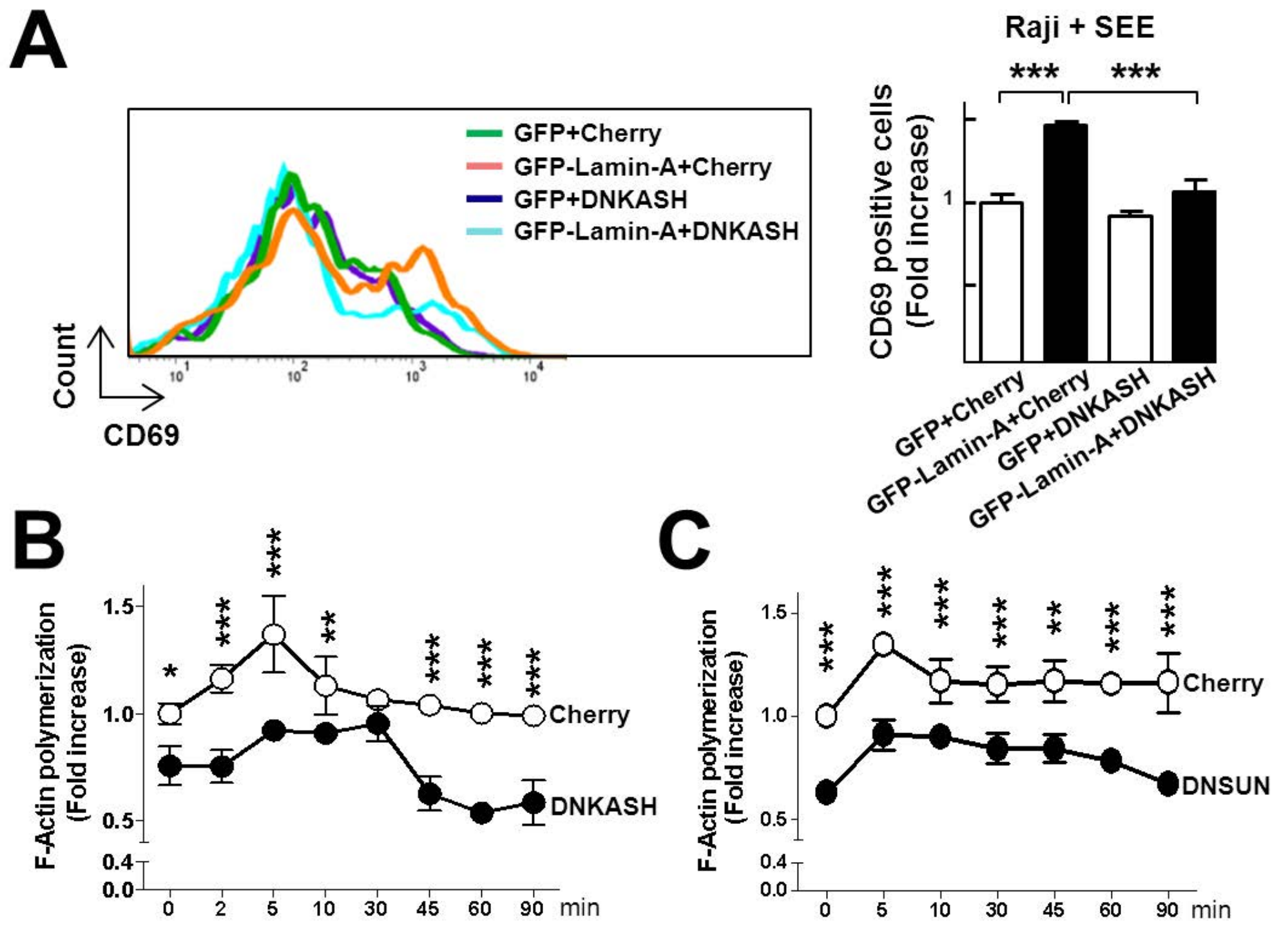
A
GFP+Cherry
GFP-Lamin-A+Cherry
GFP+DNKASH
GFP-Lamin-A+DNKASH
Count
CD69
Raji + SEE
***
***
CD69 positive cells
(Fold increase)
1
GFP+Cherry
GFP-Lamin-A+Cherry
GFP+DNKASH
GFP-Lamin-A+DNKASH
B
F-Actin polymerization
(Fold increase)
1.5
1.0
0.5
0.4
0.0
*
***
***
**
***
***
***
Cherry
DNKASH
0
2
5
10
30
45
60
90
min
C
F-Actin polymerization
(Fold increase)
1.5
1.0
0.5
0.4
0.0
***
***
***
***
**
***
***
Cherry
DNSUN
0
5
10
30
45
60
90
min